ACS APPLIED MATERIALS & INTERFACES

www.acsami.org

Research Article

Trail Formation Alleviates Excessive Adhesion and Maintains Efficient Neutrophil Migration

Wenhui Hu, Wenbo Gao, Yixin Gong, Pan Guo, Wang Li, Xinyu Shu, Shouqin Lü, Zhu Zeng, Yan Zhang,* and Mian Long*

Cite This: *ACS Appl. Mater. Interfaces* 2023, 15, 17577−17591

Read Online

ACCESS | Metrics & More | Article Recommendations | Supporting Information

ABSTRACT: Migrating neutrophils are found to leave behind subcellular trails *in vivo*, but the underlying mechanisms remain unclear. Here, an *in vitro* cell migration test plus an *in vivo* observation was applied to monitor neutrophil migration on intercellular cell adhesion molecule-1 (ICAM-1) presenting surfaces. Results indicated that migrating neutrophils left behind long-lasting, chemokine-containing trails. Trail formation tended to alleviate excessive cell adhesion enhanced by the *trans*-binding antibody and maintain efficient cell migration, which was associated with differential instantaneous edge velocity between the cell front and rear. CD11a and CD11b worked differently in inducing trail formation with polarized distributions on the cell body and uropod. Trail release at the cell rear was attributed to membrane ripping, in which β_2-integrin was disrupted from the cell membrane through myosin-mediated rear contraction and integrin−cytoskeleton dissociation, potentiating a specialized strategy of integrin loss and cell deadhesion to maintain efficient migration. Moreover, neutrophil trails left on the substrate served as immune forerunners to recruit dendritic cells. These results provided an insight in elucidating the mechanisms of neutrophil trail formation and deciphering the roles of trail formation in efficient neutrophil migration.

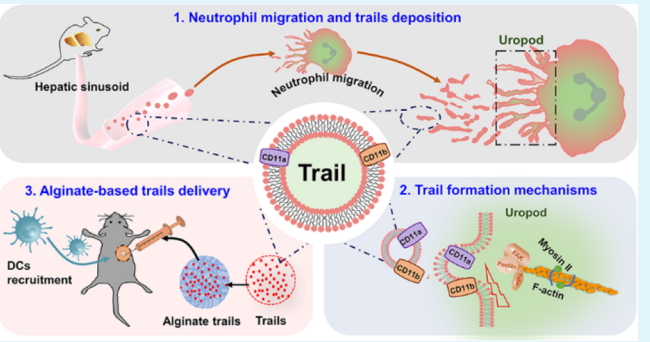

KEYWORDS: *neutrophil migration, trail release, rear contraction, β_2-integrin, cell adhesion*

INTRODUCTION

Neutrophils (polymorphonuclear cells) are the most abundant circulating leukocytes in humans, comprising the first line of host defense against invading pathogens.[1] They are also crucial to tissue damage in autoimmune diseases[2] and atherosclerosis and myocardial infarction.[3] In most inflammatory processes, neutrophils serve as the first cell type that migrates across the vascular endothelium into the tissue.[4] This multistep cascade consists of successive interactions between neutrophils and endothelial cells. Neutrophils tether to, roll over, firmly adhere to, and crawl on the endothelium followed by transendothelial migration in which leukocytes leave the bloodstream and enter the tissue sites of inflammation.[5] Evidently, efficient migration capability is required for neutrophils to clear pathogens,[6] remodel local immune microenvironments,[7] and signal for the subsequently immune cells[8,9] following infection.

β_2-Integrins, composed of a common β_2 subunit with unique α subunit (CD11a-d) as noncovalently heterodimers, are a family of myeloid cell-specific adhesion molecules specifically expressed on leukocytes.[10] CD11a and CD11b are known to be essential for neutrophil adhesion, migration, and phagocytosis of microbes.[11] Patients suffering from leukocyte adhesion deficiency type I (LAD I), an inherited defect of CD11a and CD11b, show a severe impairment of neutrophil recruitment to the sites in recurrent bacterial infections.[12] During inflammation, the endothelial membrane protein intercellular cell adhesion molecule-1 (ICAM-1) is upregulated,[13] allowing neutrophil adhesion to the endothelium by integrin−ligand interaction. Binding of CD11a or CD11b to their endothelial counterligand ICAM-1 generates survival cues for neutrophils.[14] Furthermore, ligand-specific binding forces of CD11a and CD11b imply diverse roles of β_2-integrins in neutrophil recruitment[15] and determine the direction of neutrophil migration along the activated endothelium.[16] In addition, CD11a in humans is more rapidly activated than CD11b, but CD11a activation is more transient, being deactivated after 1 min.[17] This may reflect different roles of CD11a and CD11b in transendothelial migration, where CD11a facilitates slow rolling and early adhesion whereas

Received: January 9, 2023
Accepted: March 16, 2023
Published: March 28, 2023

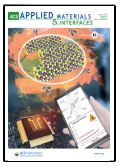

https://doi.org/10.1021/acsami.3c00288
ACS Appl. Mater. Interfaces 2023, 15, 17577−17591

CD11b has a more prominent role during firm adhesion.[11] Exceptionally, unlike the capillary endothelium of most other tissues, the adherence of neutrophils in liver sinusoids is context-dependent. In sterile inflammation, β_2-integrin−ICAM-1 interactions are required for adherence, but interactions of endothelial-cell-expressed hyaluronan with neutrophil-expressed CD44 also occur during infection in addition to β_2-integrin−ICAM-1 interactions.[18] For example, IL-10 is released in the infected liver and decreases neutrophil β_2-integrin expression, allowing for CD44-mediated adhesion.[19]

Understanding cell migration features is critical for the development of biomaterials for advanced medical device, as demonstrated, for instance, by the first clinical percutaneously implanted left atrial appendage occluder using a cutting-edge technique of surface modification to enhance cell migration based on the in-depth fundamental research of cell−material interactions.[20] Cell adhesion to the extracellular matrix (ECM) or a relevant biomaterial is a prerequisite for cell migration and mediated by adhesion receptors including integrins or by other ways.[21−23] Cell migration is a complex translocation process *via* spatiotemporal coordination of multiple events such as actin assembly-driven lamellipodium extension, myosin-powered cytoskeletal contraction, and rear detachment.[24,25] To maintain persistent migration, cell-substrate adhesions need to be continuously formed at the cell front and disrupted at the cell rear to allow for cell locomotion.[24,26] Thus, the dynamic behaviors of integrins at the rear of the cell is important in governing rear release and determining migrating velocity for various cell types.[25] For example, a "membrane ripping" usually occurs to release cell-substratum attachments during cell rear detachment for slowly migrating cell types, including fibroblasts,[27] keratinocyte,[28] and cancer cells.[29,30] In this process, a major fraction of integrin-containing membranous patches tends to remain on the substrate in the form of characteristic "migration tracks".[28,31] For those neutrophils that migrate more rapidly and persistently, however, they seem not to expend vast quantities of integrins as observed in fibroblast migration.[28] Recently, migrating neutrophils were also found to leave behind long-lasting membranous trails that are enriched in the chemokine CXCL12.[8,32] As hapatokinetic signals,[8,9] these trails were generated from neutrophils migrating across the vessel wall or in the tissue. Unfortunately, the mechanisms of how the trail is formed in rapidly migrating cells remain unclear.

In this study, an *in vitro* model was developed to elaborate the neutrophil migration onto the intercellular adhesion molecule 1 (ICAM-1)-immobilized substrate together with subtle *in vivo* observations. Integrin-enriched membranous trails alleviated excessive adhesion and maintained efficient cell migration, which is mainly governed by β_2-integrin-dominated cell adhesion. Trail formation resulted from the mechanical disruption of the cytosolic CD11b tail linking to F-actin and was enhanced by *trans*-binding anti-neutrophil antibodies. Respective contributions of CD11a and CD11b and related intracellular signaling pathways were also discussed.

MATERIALS AND METHODS

Reagents and Antibodies. Recombinant mouse (796-IC) ICAM-1-Fc chimera proteins were purchased from R&D Systems (Minneapolis, MN, USA). Histopaque-11191 and -10771, ethylene diamine tetraacetic acid (EDTA), ethylene glycol tetraacetic acid (EGTA), blebbistatin (myosin II inhibitor), glucono delta-lactone (GDL), sodium alginate, and calcium carbonate ($CaCO_3$) were from Sigma-Aldrich (St. Louis, MO, USA). Protein G and rhodamine phalloidin were from Abcam (Cambridge, MA, USA). Fetal bovine serum (FBS), cell tracker fluorescent probes, CellMask Green or Red, and Alexa Fluor 488-conjugated wheat germ agglutinin (WGA) were from Thermo Fisher Scientific (Waltham, MA, USA). Recombinant mouse granulocyte-macrophage colony stimulating factor (rmGM-CSF) and recombinant human interleukin-4 (rmIL-4) were from Peprotech (Rocky Hill, NJ, USA). RPMI medium modified with GlutaMax, Hank's balanced salt solution without phenol red (HBSS), and Dulbecco's phosphate-buffered saline (DPBS) were from GE Healthcare Life Sciences (Logan, UT, USA). Mouse CCL6 enzyme-linked immunosorbent assay (ELISA) kits and mouse CXCL12 ELISA kits were from Solarbio (Beijing, China). Mouse chemokine and cytokine arrays were from R&D systems (Tustin, CA, USA).

Alexa Fluor 647-conjugated anti-mouse Ly6G (1A8), FITC-conjugated anti-mouse CD11b (M1/70), FITC-conjugated anti-mouse CD11a (M17/4), FITC-conjugated anti-mouse CD44 (IM7), FITC-conjugated anti-mouse CD54 (YN1/1.7.4), FITC-conjugated anti-mouse CD45 (30-F11), Alexa Fluor 647 or APC-conjugated anti-mouse CD11c (N418) antibodies (Abs), and the corresponding isotype-matched FITC-conjugated anti-mouse IgG2a (RTK2758) or anti-mouse IgG2b (RTK4530) Abs were from BioLegend (San Diego, CA, USA). Rabbit monoclonal Ab against mouse FAK (EP695Y) or mouse paxillin (Y113), rabbit polyclonal Ab against mouse talin1, Alexa Fluor 647-conjugated goat polyclonal Ab against rabbit IgG, and Alexa Fluor 488-labeled goat polyclonal Ab against rat IgG were from Abcam (Cambridge, MA, USA).

Antibody Cleavage and SDS-PAGE Blotting. For Fab and Fc cleavage, rat Abs to Ly6G (1A8), CD11a (M17/4), and CD11b (M1/70) were purchased from BioLegend (San Diego, CA, USA). The Fab preparation kit was from Thermo Fisher Scientific (Waltham, MA, USA). Two hundred micrograms of each Ab was digested for 6 h with immobilized papain according to the manufacturer's protocol. The purity of the resulted Fab and Fc preparations was verified by SDS-PAGE blotting. Briefly, the blotting was performed with gels containing 12% acrylamide. The gels were stained with Coomassie R-250 staining (according to the Bio-Rad protocol, with 0.1% Coomassie blue, 10% acetic acid, and 20% methanol) for 2 h and destained in 10% acetic acid for 4 h followed by washing in H_2O for 10−15 min. Collected gels were photographed using a Nikon camera (Tokyo, Japan).

Isolation and Culture of Primary Cells. Mouse neutrophils or dendritic cells (DCs) were isolated from a 6- to 8-week-old, male C57BL/6 mouse using density gradient media Histopaque-11191 and Histopaque-10771, as described.[33] Briefly, neutrophils from mouse bone marrow were isolated by Histopaque density gradient centrifugation at 700*g* for 30 min, and the neutrophil-enriched layer was collected and washed by DPBS with 1% (w/v) BSA at 300*g* for 10 min. Isolated neutrophils were suspended in ice-cold DPBS and kept on ice until use. Collected cells were used within 3 h after isolation, and the cell concentration was determined using a hand-held cell counter (Scepter 2.0, Millipore, Germany) to be 5×10^5 cells/mL. In some cases, neutrophils were pretreated with 50 μM blebbistatin for 15 min on ice followed by live cell migration imaging for 10 min. Here, the blebbistatin was dissolved in DMSO when the blank DMSO served as control.

To isolate mouse DCs, the bone marrow was flushed using RPMI 1640 containing 2% FBS. The cell suspension was centrifuged at 300*g* for 5 min and resuspended in the red blood cell lysis buffer for 5 min to remove the remaining red blood cells. After washing in RPMI 1640/2% FBS, collected cells were suspended in DC culture media (RPMI 1640, 10% FBS, penicillin/streptomycin, GlutaMax, 20 ng/mL GM-CSF, and 10 ng/mL IL-4) at a concentration of 10^6 cells/mL. The identity and purity of DCs were verified using the $CD11c^+$ biomarker by flow cytometry after an additional 6 day culture for DC differentiation prior to adding onto the ICAM-1 substrate with α-Ly6G-stained neutrophils.

Preparation of Cell Migrating Surfaces. Coverslips were coated with 10 μg/mL of mouse ICAM-1-Fc chimeras for 60 min

https://doi.org/10.1021/acsami.3c00288
ACS Appl. Mater. Interfaces 2023, 15, 17577−17591

at 37 °C following the precoating of 100 μg/mL of protein G at 4 °C overnight. Extra ICAM-1s on the coverslips were removed, and the validity of their physical absorption was identified by staining with FITC-conjugated anti-CD54 Abs. BSA (1%) was then incubated on the substrate for 30 min at 37 °C prior to adding the neutrophils prestained with the respective Abs against Ly6G or CD11b. In some cases, to test the roles of antibody immobilization, soluble Ly6G Abs were also absorbed physically on the substrate surface and then confirmed using immunostaining with their respective fluorescent Abs. Here, a high concentration of 3% BSA was then used to block fully those free sites on the substrate for 30 min at 37 °C prior to adding the neutrophils prestained with the respective Abs, and mean fluorescence intensity (MFI) was measured in various cases for comparisons.

Live Cell Imaging and Analysis of Neutrophil Migration and Trail Formation. Cells were grouped into either intact cell with no antibody staining or stained cells with Alexa Fluor 488 anti-Ly6G Ab (shortened as α-Ly6G). Both Alexa Fluor 488 α-Ly6G-stained cells (15 μg/mL) and intact cells were labeled by the cell tracker (0.5 μM) at 4 °C for 15 min. A total of 5×10^5 isolated neutrophils were added to the ICAM-1-immobilized surfaces at 37 °C and allowed to adhere and spread for 5 min before imaging. After washing in PBS five to seven times, the cells adhered on the surfaces were incubated with prewarmed HBSS (with Ca^{2+} and Mg^{2+}). To calculate multicellular migration average velocity, time-lapsed differential interference contrast (DIC) imaging was captured separately at 30 s intervals for 15 min using an IX81 automatic inverted microscope (Olympus, Tokyo, Japan) equipped with an electron-multiplying charge-coupled device camera (iXon Ultra 897, Andor, UK). The experiments were conducted in a custom-made heating device, with temperature control (37 ± 0.5 °C) and 5% CO_2 supply, during live cell imaging. Time-lapsed trajectories of migrating cells were first monitored using the Manual Tracking Plugin Tool of the ImageJ software. The velocity of a cell was then calculated using Chemotaxis and Migration Tool 2.0 (IBIDI, Martinsried, Germany) upon moving distance of the centroid of the cell per unit time, and the multicellular average velocity was obtained from all the cells in typical three to five fields per test, except those being overlapped or contacted with neighboring cells.

For single cell migration analysis, especially for instantaneous contraction and protrusion velocities, time-lapsed immunofluorescence imaging was then captured at 30 s intervals for 15 min by confocal laser scanning microscopy (LSM880 NLO, Zeiss, Oberkochen, Germany) with a 63×/0.95NA objective. The trajectories of the rearmost and frontmost edges of a cell were monitored, and the velocities were then calculated, as mentioned above, to represent the instantaneous contraction and protrusion velocities, respectively, at each time point of the migrating cell.

Fixed Cell Microscopy and Image Analysis. The structures of neutrophil trails were observed and analyzed using scanning electron microscopy (SEM, SU8010, Hitachi, Japan) and confocal laser scanning microscopy (LSM880, Zeiss, Oberkochen, Germany) with a 63×/0.95NA objective. For SEM observations, neutrophils were fixed in 2.5% glutaraldehyde and dehydrated with graded ethanol. Critical point drying was performed using carbon dioxide in a Leica EMCPD300. After coating with gold, the samples were visualized. For confocal microscopic observations, cells were fixed in 3.7% formaldehyde solution at room temperature for 20 min and permeabilized with 0.1% Triton X-100 for 5 min. To label cell membrane WGA or surface-bound CD11a, CD11b, CD44, or Ly6G, the cells were incubated, respectively, with Alexa Fluor 488 conjugated-WGA (5 μg/mL), Alexa Fluor 488 anti-CD11a (50 μg/mL), Alexa Fluor 488 anti-CD11b (50 μg/mL), Alexa Fluor 488 anti-CD44 (50 μg/mL), or Alexa Fluor 647 anti-Ly6G (50 μg/mL) Ab at 37 °C for 20 min before permeabilization. To label the cell cytoplasm, neutrophils were incubated with cell tracker fluorescent probes (0.5 μM) at 4 °C for 15 min before adding the cells onto the migrating surfaces.

To quantify trail formation, cells were labeled by WGA (5 μM) for the cell membrane and by rhodamine phalloidin (165 μM) for intracellular actin after cell fixation. Trail formation ratio, denoting the fraction of migrating cells presenting the trails, was calculated by the number of cells with trails to the total cell number from randomly selected 8−10 fields with a total of 30−50 cells each field. Trail area was obtained by image binarization using the MATLAB (Mathworks, Natick, MA) software and contoured region calculated on the codes self-programmed in the Supporting Information. Trail length was measured using the Length Measurement Tool of the ImageJ software based on the definitions for the straight distance between the endpoint of the uropod and the farthest end of the trail. All these parameters were calculated for all the cells per test except for those cells overlapped with neighboring cells, and three tests were repeated in each case. To quantify the cytoskeletal distribution, the stained cytoskeleton was segregated into the front and rear regions on the bisector of the cell perpendicular to the direction of migration, and the MFI ratio of the cell front to the cell rear was then estimated. This MFI ratio less than or equal to unity was termed as F-actin rear enrichment. Also, the F-actin rear enriched ratio was defined as the fraction of cells showing F-actin rear enrichment in view.

Collection and Characterization of Isolated Trails. Neutrophils were allowed to migrate on ICAM-1-immolobilized coverslips for 60 min. After being washed by DPBS three times, both adhered neutrophils and remnant trails were harvested using a cell scraper. Those neutrophils in the mixture suspension were removed by centrifugation at 1000*g* for 30 min, and the remaining supernatant was further centrifuged at 18,000*g* for 60 min to collect the remaining trails, as described in the literature.[8] To identify the surface molecules and cytoplasmic components of these isolated trails, immunofluorescence analysis was conducted by allowing the trails to adhere and migrate onto ICAM-1-coated coverslips. To label surface-bound β_2-integrin or Ly6G of the trails, the cells were preincubated with Alexa Fluor 488 conjugated-β_2-integrin CD18 (50 μg/mL) and Alexa Fluor 647 anti-Ly6G (50 μg/mL) Ab, respectively, at 37 °C for 20 min before adding the cells onto the migrating substrates. To label cytoplasmic components of the trails, neutrophils were preincubated with cell tracker fluorescent probes (0.5 μM) at 4 °C for 15 min before adding the cells onto the migrating substrates.

The morphology and size distributions of the isolated trails were determined by transmission electron microscopy (TEM, HT-7700, Hitachi, Japan) and ZetaView (Particle Metrix, Meerbusch, Germany), respectively. The trails were loaded onto the copper grids and stained by uranyl acetate for imaging by TEM at 80 kV. For size distribution analysis, the trails were suspended in PBS and measured using nanoparticle tracking analysis (NTA) at VivaCell Biosciences with ZetaView PMX 110 and the corresponding software ZetaView 8.04.02. Meanwhile, mass spectrometric analysis was applied to identify trail components. Briefly, samples were digested with sequencing grade trypsin, and peptides were dissolved in liquid chromatography mobile phase A and separated using the EASY-nLC 1000 ultra-high-performance liquid system. Mobile phases A and B are the aqueous solutions containing 0.1% formic acid and 2% acetonitrile and containing 0.1% formic acid and 90% acetonitrile, respectively. Liquid phase gradient was set as 0−90 min, 5%−25% B; 90−112 min, 25%−35% B; 112−116 min, 35%−80% B; and 116−120 min, 80% B, and the flow rate was maintained at 500 nL/min. The peptides were separated by an ultra-high-performance liquid phase system, injected into an NSI ion source for ionization, and then analyzed by Q Exactive Plus (Thermo Fisher Scientific) mass spectrometry.

For the cytokine array test and ELISA analysis, packed trails and cell bodies were lysed by 0.1% Triton-containing DPBS supplemented with 1 mM EDTA. For comparison, 200 μg of trails and 200 μg of cell bodies were collected and quantified using the BCA Protein Assay Kit. A mouse cytokine array test was carried out using the Proteome Profiler Mouse Cytokine Array Kit (R&D Systems) according to the manufacturer's instructions. A total of 25 cytokine proteins were tested, as follows: CCL21, CXCL13, CCL6, C5/C5a, CCL28, Chemerin, CCL27, CXCL16, CCL11, CX3CL1, IL-16, CXCL10, CXCL11, CCL2, CXCL1, GCP-2, CCL8, CCL12, CCL22, CXCL9, CCL3/4, CCL9/10, CXCL2, CCL5, and CXCL12. The expression levels of CCL6 and CXCL12 in trails and cell bodies were further

https://doi.org/10.1021/acsami.3c00288
ACS Appl. Mater. Interfaces 2023, 15, 17577−17591

specified using ELISA kits (Solarbio, Beijing, China). Briefly, the lysed supernatant was collected and then centrifuged at 13,400*g* for 5 min. The supernatant or standard sample (100 μL) was added into a 96-well plate precoated with anti-mouse CCL6 and CXCL12 primary antibodies. The plate was examined at 450 nm using the iMark microplate reader (BIO-RAD, Hercules, CA, USA). A four-parameter standard curve was obtained using the absorbance ratio of the yellow product to the value of the standard sample, as per the manufacturer's instructions.

FTIR Measurements. α-Ly6G-stained mouse neutrophils were allowed to spread and migrate on ICAM-1-immobilized coverslips for 30 min at 37 °C. The coverslips were then transferred to 4 °C and washed twice with ice-cold PBS containing 2 mM EGTA and EDTA. The cell bodies were trypsinized and transferred to the CaF_2 crystals for FTIR analysis. Those stained cells directly added onto ICAM-1 coverslips without migration served as control. The water in the cell suspension was evaporated until the formation of a 2−3 mm thick film in the window. The measuring parameters were set to be the scanning range of 800−4000 cm^{-1} and the resolution of 8 cm^{-1} by scanning the stack with added samples up to128 times. All the spectra were subtracted from the blank control, and Fourier self-deconvolution was applied to detect the infrared absorption spectra.

Fluorescence Recovery after Photobleaching (FRAP) Assay. α-Ly6G-stained neutrophils were allowed to spread on ICAM-1-immobilized coverslips for 5 min at 37 °C. The coverslips were then transferred to 4 °C, and fluorescence-labeled Ab against CD11a or CD11b was added at 10 μg/mL for 10 min. The labeling medium was then removed, and the cells were washed and maintained in prewarmed HBSS. The FRAP test was performed using a laser-scanning confocal microscope (LSM880, Zeiss, Oberkochen, Germany). A 2 μm diameter circular area was photobleached, and images were captured at 0.2 fps for 100 s. The mobile fraction (the maximal percentage of initial fluorescence intensity that has been recovered up to the plateau) was estimated based on the best fit to a single exponential curve that has been reset through the origin,[34] and the diffusion coefficient (D) based on the half time required to reach the maximal recovery ($T_{1/2}$) and the original bleach area diameter (W) was calculated using the equation $D = W^2/(4T_{1/2})$.[35]

Preparation of the Alginate Hydrogel Incorporating Trails and Controlled Release of Incorporated Trails. Sodium alginate powder was dissolved in PBS to form the sodium alginate solution at room temperature. $CaCO_3$ in combination with GDL was used as a source of calcium ions to initiate gelation.[36] The molar ratio of calcium ion to carboxyl was 0.18, and a $CaCO_3$ to GDL molar ratio of 0.5 was always maintained to achieve a neutral pH value. The sodium alginate solution was added to the $CaCO_3$ suspension and mixed at room temperature for 1 h. The trails collected as described above were then added into the alginate solution with $CaCO_3$ and mixed evenly. For comparison, blank alginate hydrogels without trails were prepared in DPBS with the same volume. A fresh aqueous GDL solution was then added to the suspension and vortexed for 1 min to initiate gelation. The samples with a final concentration of 1.5% (w/v) alginate were incubated at 37 °C for 5 min to form alginate hydrogels. The dissolving reagent for alginate hydrogels was a solution mixture of 1 mM EDTA and 5 mM sodium citrate solution.[37]

For trail release tests, 500 μL of the alginate hydrogel incorporating 500 μg of trails was incubated in 250 μL of DPBS (37 °C, 5% CO_2 atmosphere). For comparison, 500 μg of trails was resuspended directly in 250 μL of DPBS. The supernatant with released trails was collected, and fresh DPBS was added every time point. The concentration of trails released into the medium was determined by the BCA Protein Assay Kit.

Animal Experiments and Immunofluorescence Staining. The experimental protocol for animal tests was approved by the Institutional Animal and Medicine Ethical Committee at the Institute of Mechanics of the Chinese Academy of Sciences. Liver intravital microscopy was performed on a 6- to 8-week-old, male C57BL/6 mouse (Vital River Laboratories, Beijing, China) as described.[38] Briefly, the mouse was anesthetized (10 mg/kg xylazine hydrochloride and 200 mg/kg ketamine hydrochloride) *via* intraperitoneal injection. Mouse body temperature was maintained using a heating pad. The mouse was placed down on its right side to expose the liver. To avoid jitter caused by mouse breathing, the liver ligaments were clipped, and the xiphoid was fixed on heating pad. To stain neutrophils *in vivo*, 2 μL (1 μg) of anti-Ly6G-Alexa Fluor 647 monoclonal Ab (1A8; BioLegend) was diluted in 100 μL of PBS and injected from the tail vein at 30 min before imaging. Images were acquired with confocal laser scanning microscopy (LSM880 NLO, Zeiss, Oberkochen, Germany).

The alginate hydrogel was injected into a 6- to 8-week-old, male C57BL/6 mouse. Briefly, the mouse was anesthetized (10 mg/kg xylazine hydrochloride and 200 mg/kg ketamine hydrochloride) *via* intraperitoneal injection. The mouse was subcutaneously injected at two sites of the dorsal side with 100 μL of the blank alginate hydrogel and 100 μL of the alginate hydrogel incorporating 100 μg of trails, respectively. The alginate hydrogels were harvested at 48 h to assess the DC recruitment. For immunological staining, alginate hydrogels were fixed by 4% paraformaldehyde and then were blocked by 5% (v/v) BSA for nonspecific absorption. Then, the hydrogels were incubated with APC-CD11c for 24 h at 4 °C and washed by DPBS for at least six times. The hydrogels were scanned using confocal laser scanning microscopy (LSM880 NLO, Zeiss, Oberkochen, Germany), and the number of fixed DCs was counted in a fixed scan area (2.2×10^6 μm^3) of hydrogels.

Flow Cytometry Analysis. Flow cytometry was performed using a FACS Calibur cytometer (BD Biosciences, NJ, USA). Isolated mouse neutrophils were incubated with anti-CD11b, -CD11a, or -Ly6G Abs at 10 μg/mL in DPBS buffer on ice for 20 min when isotype-matched Abs served as control. For those *in vivo* DC recruitment analyses, the subcutaneous hydrogels were harvested and dissolved by 1 mM EDTA and 5 mM sodium citrate solution. All the leukocytes were collected and labeled by FITC-CD45 and APC-CD11c at 10 μg/mL in DPBS buffer on ice for 20 min when isotype-matched Abs served as control. After washing in DPBS, the cells were resuspended in DPBS and analyzed by flow cytometry.

DC Recruitment Imaging and Chemotaxis Assay. For live DC imaging *in vitro*, α-Ly6G-stained mouse neutrophils were allowed to spread and migrate on ICAM-1-immobilized coverslips for 30 min at 37 °C. The coverslips were then transferred to 4 °C and washed twice with ice-cold PBS until use. Differentiated DCs for 6 days were prelabeled separately with CellMask Red for 15 min at 4 °C. A total of 10^6 DCs were added to the substrate after allowing neutrophils migrating for 30 min and then DCs adhering for 1−2 min before imaging. Time-lapsed immunofluorescence images were captured at 30 s intervals for 1 h by confocal laser scanning microscopy (LSM880 NLO, Zeiss, Oberkochen, Germany) with a 63×/0.95NA objective. The number of adhered DCs on neutrophils' premigrated substrate was counted and normalized to the DC number on ICAM-1 substrate alone.

For *in vitro* DC chemotaxis assay, cells were placed onto the upper chamber of a Transwell plate (5 μm pore size, Corning, NY, USA). The lower chamber was filled with the same volume with the suspensions of trails, blank alginate hydrogels, or trail alginate hydrogels (*i.e.*, 100 μL of hydrogels with 100 μg of trails or 100 μL of blank hydrogels). The number of transmigrated DCs from the upper to the lower chamber was counted at 24 h and normalized to the total DCs in the upper chamber.

Statistical Analysis. Error bars depicted the standard errors of the mean (SEMs), and all data were presented as the mean ± SEM. A Student t test or Mann−Whitney test was performed depending on whether the data pass the normality test for two-group comparison. One-way ANOVA test followed by the Newman−Keuls test was used for multiple-group comparison when the data pass the normality test, whereas the nonparametric Kruskal−Wallis test followed by Dunn's test was applied when the data fail to pass the normality test. All statistical analyses were performed using the Prism statistical software (GraphPad Software, CA, USA). $p < 0.05$*, 0.01**, 0.005***, and 0.0001****.

https://doi.org/10.1021/acsami.3c00288
ACS Appl. Mater. Interfaces 2023, 15, 17577−17591

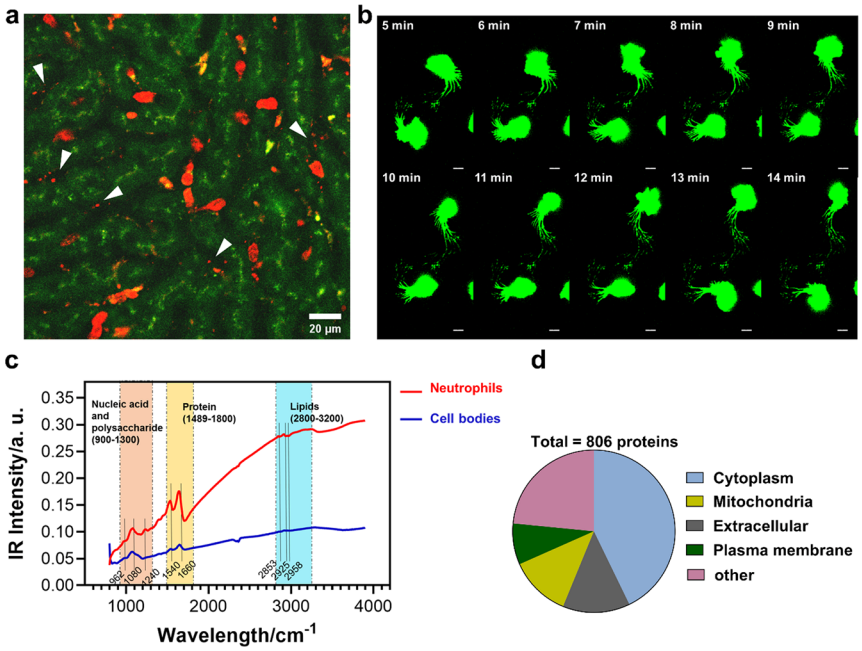

Figure 1. α-Ly6G-stained neutrophils leave behind long-lasting, chemokine-containing trails. (a) A typical *in vivo* image of α-Ly6G-stained neutrophils (*red*) migrating on mouse liver sinusoids (*green*, liver autofluorescence) at t = 30 min after α-Ly6G antibody injection from the tail vein (also refer to Video S1). *Arrows* indicate the massive subcellular structures deposited by migrating neutrophils. Scale bar, 20 μm. (b) Time-lapsed images showing an α-Ly6G-stained (*green*) neutrophil migrating on ICAM-1-immobilized substrate (also refer to Video S2). Scale bar, 5 μm. (c) Fourier transform infrared spectrometer analysis for compositional differences between entire neutrophils (premigration) and remaining cell bodies (postmigration without trails). (d) Mass spectrometric analysis of isolated trails.

Data Availability. All data needed to evaluate the conclusions are present in the paper and/or the Supporting Information. Additional data related to this paper may be requested from the authors.

RESULTS

Migrating Neutrophils Leave behind Long-Lasting, Chemokine-Containing Trails. We first conducted *in vivo* tests to visualize neutrophil migration in the mouse liver. Ly6G$^+$ neutrophils stained by Alexa Fluor 647-conjugated α-Ly6G antibodies migrated along hepatic microcirculation and deposited massive subcellular structures on liver sinusoids over the first hours (Figure 1a, Video S1). These vesicle-like structures left behind migrating neutrophils and were deposited onto the hepatic sinusoidal lumen. To further characterize these subcellular structures, an *in vitro* migration assay was developed by placing α-Ly6G-stained mouse neutrophils onto ICAM-1-immobilized coverslips to mimic *in vivo* neutrophil migration on sinusoids because ICAM-1 is constitutively expressed on the sinusoids, resulting in hepatic adhesion of flowing neutrophils mediated by ICAM-1−β_2-integrin interaction.[39] Time-lapsed live imaging demonstrated that migrating neutrophils presented a featured morphology with a ruffled leading edge at the front, a thick cell body at the middle, and an elongated uropod full of retracting fibers at the rear of the cell. The cell left behind long-lasting membranous trails from the uropod during persistent migration (Figure 1b, Video S2) and can be segregated into three subcellular regions of *cell body*, *uropod*, and *trails* (Figure S1a). SEM imaging indicated that the trails are discontinuous structures containing numerous small vesicles attached to the substrates (Figure S1b). Strong cell tracker signals within the trails suggested that these small vesicles are enclosed membranous structures with wrapped cytoplasm inside the trails (Figure S1c). As adhesion molecules (*i.e.*, CD11a, CD11b, and CD44) and cytoskeleton or focal adhesion proteins (*i.e.*, F-actin, FAK, paxillin, and talin) are key in initiating neutrophil adhesion and migration,[22,26,40] further examination of these proteins' distributions on trails indicated that CD11b and CD11a were apparently present (Figure S2a), but F-actin, CD44, and the three focal adhesion proteins were rarely observed (Figure S2b). To elucidate the intrinsic compositions of the trails, the cell body and the trails originated from migrating neutrophils on ICAM-1 were isolated, respectively.

Immunofluorescence analysis was conducted *via* staining surface molecules and cytoplasmic components of trails on ICAM-1-coated coverslips. Results indicated that the trails are β_2-integrin-presenting, cytoplasm-containing membranous vesicles and could attach to the ICAM-1 substrate (Figure S3a−c). The morphology and size distribution of isolated trails were tested by transmission electron microscopy (TEM) (Figure S4a) and ZetaView (Particle Metrix, Germany) (Figure S4b), respectively, presenting that the trails exhibited a typical vesicular structure peaked with a diameter of approximately 130 nm. Fourier transform infrared analysis indicated that the cell body of neutrophils after trail release lost massive lipids compared to those intact cells (Figure 1c, Table S1). Composition analysis *via* mass spectrometry (Figure 1d) also indicated that trails contain abundant cytoplasmic components plus mitochondria. As cytoplasmic components were enriched in trails, their chemokine composition was screened and characterized using the mouse chemokine microarray (Figure S4c). Data showed that CCL6 was preferentially enriched in the cell bodies and the trails, and CXCL12 was highly expressed in the trails, which is consistent with the literature.[8] ELISA analysis also supported that the cell bodies presented a higher level of CCL6 (Figure S4d), whereas the trails yielded a higher level of CXCL12 (Figure S4e). Collectively, the above observations indicated that migrating

https://doi.org/10.1021/acsami.3c00288
ACS Appl. Mater. Interfaces 2023, 15, 17577−17591

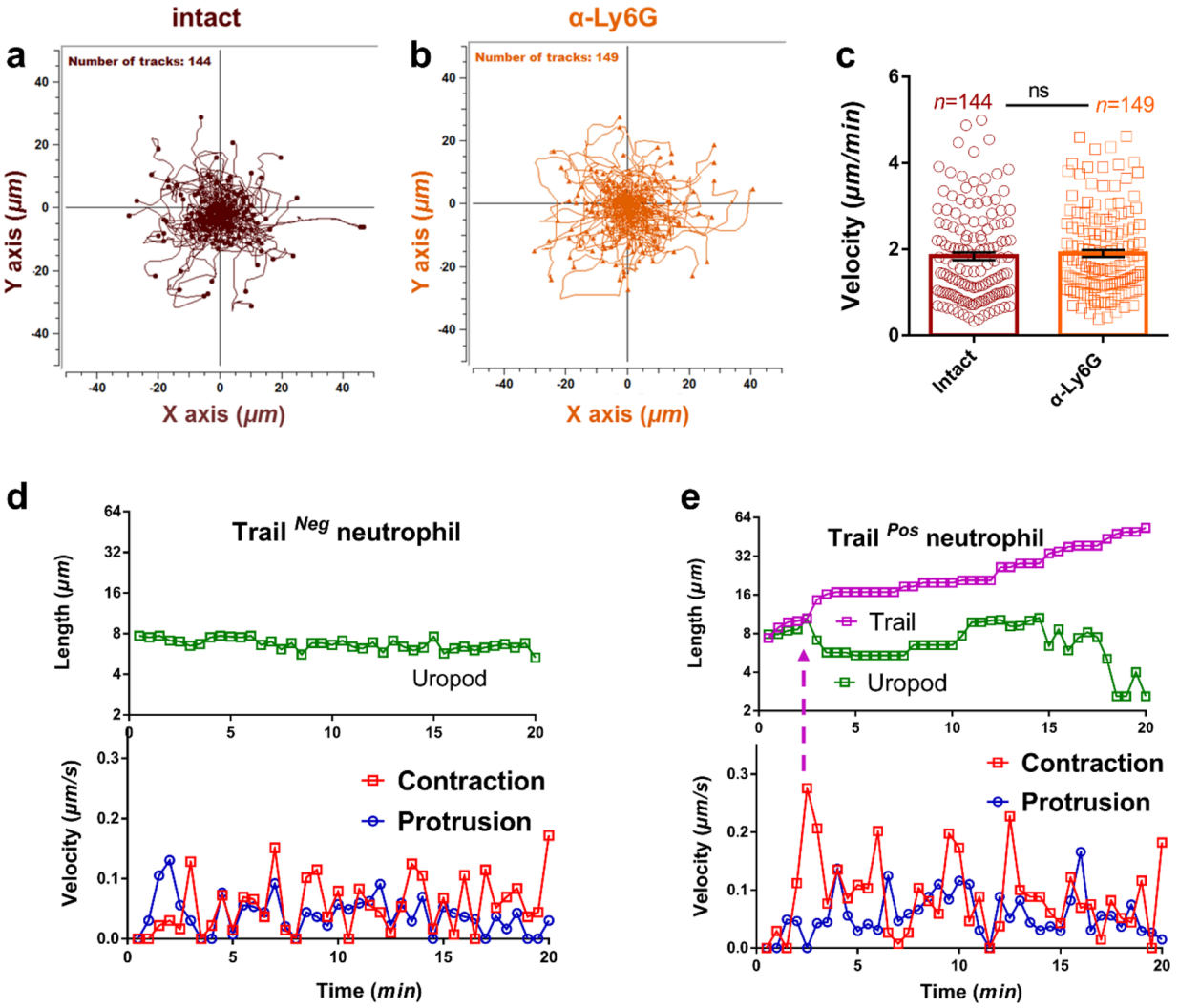

Figure 2. Migrating neutrophils with trails exhibited higher instantaneous contraction velocities. (a−c) Migration dynamics of intact (a) or α-Ly6G-stained (b) neutrophils on ICAM-1 monitored by time-lapsed microscopy for 15 min at 30 s intervals. Trajectories of 144−149 neutrophils were shown by resetting the same origins (a, b) and the average migrating velocity (c). (d, e) Time courses of uropod (*green*) or trail (*purple*) length (*upper panels*) and of instantaneous protrusion (*blue line*) or contraction (*red line*) velocity (*lower panels*) were monitored for a typical trail^{Neg} (d) or trail^{Pos} (e) cell during cell migration. Here, the instantaneous protrusion or contraction velocity was defined as the moving distance of the cell frontmost or rearmost per minute, respectively, and denoted as the polarized cell migration of the cell front or rear edge. The *pink arrow* in panel e denotes the moment that trail length started to sharply increase. Data were obtained from at least three repeats and presented as the mean ± SEM.

neutrophils were able to release long-lasting, β_2-integrin-presenting, chemokine-containing membranous trails anchored to the ICAM-1 substrate. To further confirm the above observations, experiments were repeated for intact cells to exclude the possibility of trail formation due to α-Ly6G staining itself. Cell morphology was again characterized with the cell body, uropod, and trails for intact or α-Ly6G-stained cells. The cell body and uropod were identified based on F-actin staining, and the trail was then denoted as the membranous remnants free of F-actin (Figure S5a). Unexpectedly, although the components and morphologies of the trails were quite similar between intact (Figure S6a−c) and α-Ly6G-stained cells (Figure S2a,b), the trail formation ratio of intact cells was decreased significantly, as was the case for the isotype-matched α-IgG2a-stained control (Figure S5b). Other morphological parameters including trail length (Figure S5c), area (Figure S5d), and uropod length (Figure S5e) were also remarkably decreased for intact neutrophils compared to α-Ly6G-stained cells. Thus, neutrophil trail formation was likely enhanced, but not triggered, by α-Ly6G staining during neutrophil migration.

Trail Formation Relieves Excessive Adhesion and Maintains Efficient Cell Migration. Because the trails were released from migrating neutrophils, we next examined whether α-Ly6G-staining alters neutrophil migration behaviors and thus leads to the enhanced trail formation. Comparisons of the migration capabilities between intact and α-Ly6G-stained neutrophils yielded similar cell trajectories (Figure 2a,b), resulting in comparable migrating velocities (Figure 2c) and slightly increased migrating displacement (Figure S7a) and directness (Figure S7b). Furthermore, as the fraction of migrating neutrophils with trails was observed differently in the two cases (Figure S5b), all intact and α-Ly6G-stained migrating neutrophils were further divided into two subgroups, trail^{Pos} and trail^{Neg}, to denote those cells with or without left trail, respectively. Still, no significant differences were observed between the two subgroups in average migrating velocity for either intact or stained case (Figure S8a,b).

https://doi.org/10.1021/acsami.3c00288
ACS Appl. Mater. Interfaces 2023, 15, 17577−17591

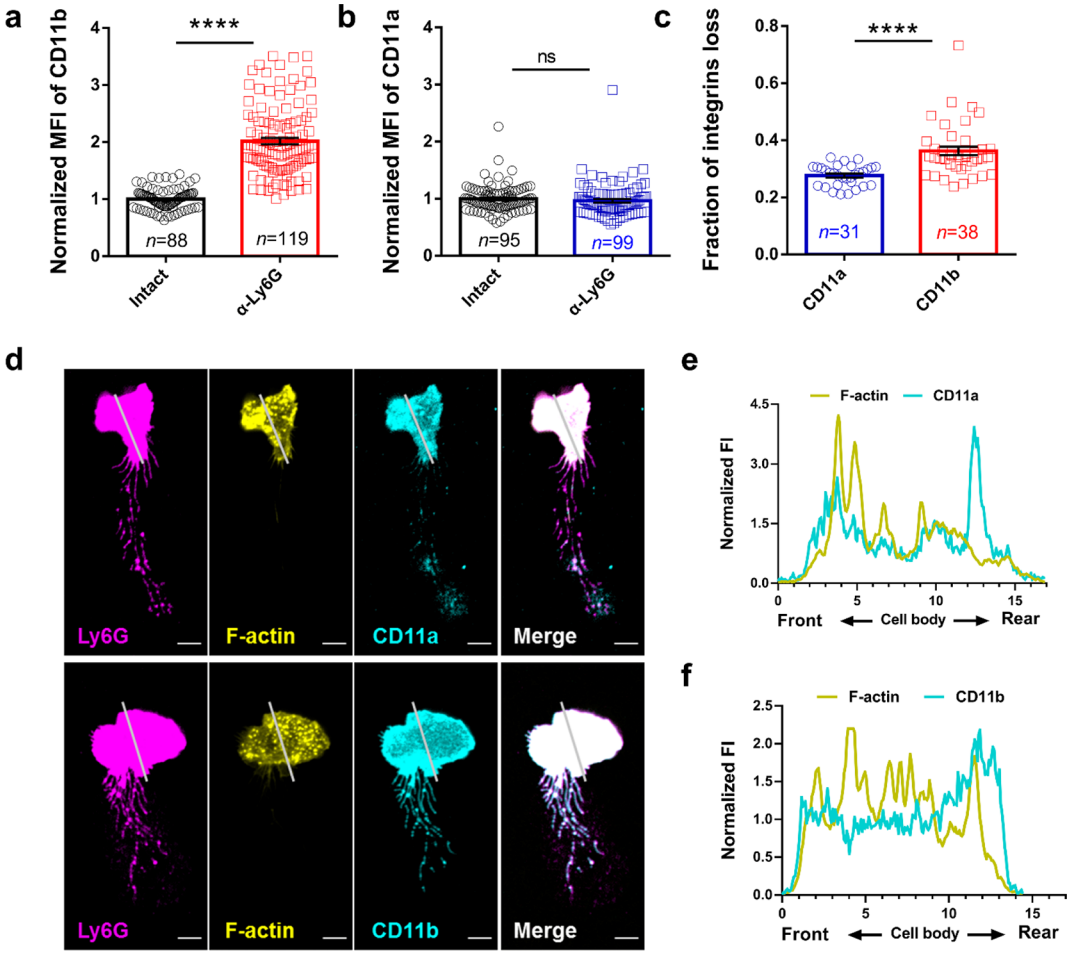

Figure 3. CD11a and CD11b work distinctively in inducing trail formation. (a–c) Expressions of CD11b (a) and CD11a (b) for α-Ly6G-stained neutrophils, normalized to the ones for intact cells, as well as fractions of CD11a and CD11b expressions on trails to the ones on cell body (c). MFI, mean fluorescence intensity. (d–f) Typical images of Ly6G (*purple*), CD11a, CD11b (*cyan*), and F-actin (*yellow*) in α-Ly6G-stained neutrophils. Scale bar, 5 μm (d). Also plotted were the fluorescence intensity profiles (in a.u.) for CD11a (e) or CD11b (f) along *gray lines* in panel d, normalized to the one from the mean fluorescence intensity of the respective fluorescence dye for CD11a- or CD11b-staining. *Yellow* and *cyan lines* indicate stained F-actin and CD11a or CD11b, respectively, in panels e and f. Data were obtained from at least three repeats and presented as the mean ± SEM; $p < 0.0001^{****}$.

Neutrophil trails tended to release from the neutrophil uropod, where the uropod was detached from the substrate to allow successive cell migration[8,32] (Figure 1b). It is still unclear how similar migrating velocities induce differential uropod and trail lengths between intact and stained neutrophils. In fact, trail formation and cell migration are coupled processes that involve at least three interdependent events: cell front protrusion, rear contraction, and uropod detachment. To explore the potential relationship of these events with cell migration dynamics, we next elaborated the velocity profiles of protrusion (cell frontmost) and contraction (cell rearmost) edges as well as the instantaneous trail and uropod lengths at the same time points. Interestingly, instantaneous protrusion or contraction velocity for trail^{Neg} neutrophils showed comparable profiles (*lower panel*), and the uropod length (*upper panel*) remained stable (Figure 2d). For trail^{Pos} neutrophils, however, the instantaneous contraction velocity presented a larger fluctuation (*lower panel*) and exhibited higher peak values compared with the instantaneous protrusion velocity from the same migrating cell (Figure 2e). Furthermore, the trail length started to increase sharply at the moment of t = 2.5 min, corresponding to the first peak of instantaneous contraction velocity, and exhibited gradual transition to reach the plateau, which was mirrored with the descending phase transition of uropod length (*upper panel* in Figure 2e). These observations suggested that a specialized migration manner, featured by differential protrusion and contraction velocities, could contribute to trail formation based on high-instantaneous velocity rear contraction.

As the actin network orchestrates the rear contraction and the cell migration,[22,41,42] we further compared intracellular actin distribution of α-Ly6G stained trail^{Pos} and trail^{Neg} neutrophils. Obviously, the intracellular F-actin network for α-Ly6G stained cells was redistributed (Figure S8c), i.e., high expression at the cell front for trail^{Neg} neutrophils and polarized accumulation at the cell front and rear for trail^{Pos} neutrophils. Statistical analyses of trail^{Neg} and trail^{Pos} neutrophils suggested the potential roles of F-actin locating at the cell rear in trail formation (Figure S8d), as it was seen that the trail formation ratio was positively correlated to the F-actin rear enrichment ratio (Figure S8e). Blebbistatin-treated neutrophils showed unchanged average migrating velocity (Figure S9a–c), decreased rear instantaneous contraction velocity (Figure S9d–f), and reduced F-actin rear enrichment ratio (Figure

https://doi.org/10.1021/acsami.3c00288
ACS Appl. Mater. Interfaces 2023, 15, 17577–17591

S10a), resulting in a dramatic attenuation of trail formation, as observed in the reduced trail formation ratio (Figure S10b), length (Figure S10c), and area (Figure S10d) with less-branched configuration (Figure S9d) and the elongated uropod (Figure S10e). Taken together, these results suggested that α-Ly6G staining helped neutrophils to accumulate actin filaments at the cell rear and promote intense contraction mediated by myosin II-induced, high-instantaneous velocity rear-end retraction, which in turn drove trail formation.

Because the uropod elongation in neutrophils is assumed to be mediated by the forces at the contact between neutrophils and endothelium and the balance between adhesion at the front and deadhesion at the rear is crucial for regulating the directed cell migration,[32,43,44] we hypothesize that the drastic rear contractility in the dynamic trail formation is probably due to the excessive adhesion and the difficulty of rear-end detachment during neutrophil migration. Indeed, uropod detachment seemed relatively difficult with the elongated uropod length for the entire α-Ly6G-stained (Figure S5e) or even trail^{Pos} (Figure S11a) cells, thus calling for the specialized migration strategy to maintain successive neutrophil migration. To test this hypothesis, we first evaluated the adhesion capability of α-Ly6G-stained cells on ICAM-1 because their trail formation capability was known to be highly elevated (Figure S5b−e). Results indicated that α-Ly6G staining significantly enhanced the cell spreading area (Figure S11b) and adherent number (Figure S11c) compared with those for intact or isotype-matched IgG2a-stained cells. Next, real-time monitoring of the cell spreading area evolution during 10 min migration indicated that the spreading area of α-Ly6G-stained cells at t = 10 min normalized to the one at t = 0 was dramatically reduced, whereas no significant difference was found in intact or isotype-matched IgG2a-stained cells (Figure S11d). As the average migrating velocity remains unchanged between intact and α-Ly6G-stained neutrophils, it is appropriate to speculate that trail release serves as a strategy for neutrophils to alleviate excessive adhesion and maintain efficient cell migration.

CD11a and CD11b Work Distinctively in Inducing Trail Formation. Because neutrophil adhesion on ICAM-1 is β_2-integrin-dependent,[11] we then tested how CD11b and CD11a work in this process. Consistent with the above findings for elevated adhesion capabilities of α-Ly6G-stained neutrophils, a significant upregulation of CD11b expression (Figure 3a) was observed, whereas CD11a expression remained unchanged (Figure 3b). Moreover, the distributing fraction of CD11b on the trails to that on the cell body was significantly higher than that of CD11a (Figure 3c), indicating the massive loss of CD11b compared with CD11a on the trails. Therefore, neutrophils tended to alleviate CD11b-engaged excessive adhesion by discarding the trails that contain abundant CD11b and bits of CD11a. To clarify the potential mechanisms of β_2-integrin discarding during neutrophil migration, a tricolored confocal imaging assay was used to elucidate their roles. Results indicated that CD11a and CD11b were mainly located at the uropod of the migrating cell (Figure 3d), seemingly serving as a "*reserve pooling*" in the dynamic rear-end retraction and trail formation. Compared to CD11b with rare colocalization with F-actin, CD11a was organized to form small punctate clusters that were partially colocalized with F-actin, implying a stronger interaction with the cytoskeleton network (Figure 3e,f). To confirm this observation, a FRAP test was conducted to estimate the mobility of CD11a and CD11b on the apical surface of migrating cells. Data showed that the recovery capability of CD11b was significantly higher than that of CD11a (Figure S12a), yielding ∼3-fold higher diffusion coefficient and mobile fraction at the same time scale (Figure S12b,c). This difference manifested the stronger mechanical strength of CD11a connecting the intracellular tail to the actin cytoskeleton. Collectively, in the cytoskeleton-mediated vigorous rear contraction, the localized abundant CD11b at the cell rear was easier to be discarded in the trail formation owing to its weaker connection to the cytoskeleton, favorable to relieving excessive adhesion and maintaining successive cell migration.

To further isolate the respective contributions of CD11a and CD11b in trail formation, we applied Fab fragments of α-CD11b and/or α-CD11a blocking antibodies in the suspension of α-Ly6G-stained neutrophils. Surprisingly, blocking CD11a but not CD11b led to a significant reduction on trail formation (Figure S13a). Meanwhile, no significant differences in trail formation capability were observed between the two cases of α-Ly6G staining alone and CD11b blocking plus α-Ly6G staining (Figure S13b−e), supporting that CD11a but not CD11b plays the dominant role in trail formation. We further explored neutrophil migration dynamics to test how CD11a regulates the trail formation. Trajectory analysis of migrating cells also showed that blocking CD11a alone or both CD11a and CD11b likely reduced the migrating capabilities of individual cells (Figure S14a), as seen in the reduced migrating average velocity (Figure S14b) and displacement (Figure S14c) as well as the enhanced directness (Figure S14d). Together, neutrophils tended to discard β_2-integrin-enriched membranous structures at the cell rear to relieve excessive adhesion and maintain successive cell migration. This specialized migration strategy relied on myosin II-mediated, vigorous rear-end retraction and CD11a-dominated migrating capability.

Enhanced Trail Formation Is Attributed to *trans*-Binding of Neutrophil-Specific Antibodies. To uncover the potential mechanisms of α-Ly6G staining-induced excessive adhesion and trail formation, we tested the dose dependence of α-Ly6G antibodies on trail formation. The trail formation ratio presented a dose-dependent manner in increasing with the concentrations of α-Ly6G antibodies (Figure S15a), confirming their role in enhancing trail formation. To further elucidate the specificity of antibody fragments, full-length α-Ly6G antibodies were digested by papain into respective Fab and Fc fragments. Interestingly, neither the Fab nor the Fc fragments alone worked effectively in trail formation (Figure 4a,b and Figure S15b,c), implying that α-Ly6G-staining-enhanced trail formation is not epitope-specific because α-Ly6G Fab fragments themselves cannot promote trail formation independently.

Thus, there are two possible ways for binding full-length α-Ly6G antibodies to neutrophils, namely, homolateral- or *cis*-binding or heterolateral- or *trans*-binding (Figure 4c). For *cis*-binding, the Fab fragments of soluble full-length antibodies are fixed to Ly6G epitopes, and the remaining free Fc fragment tends to target Fc receptors on neutrophils. For *trans*-binding, full-length antibodies are physically absorbed onto the substrate and then bind simultaneously to the Ly6G epitopes on neutrophils. To test these possibilities, the physical absorption of α-Ly6G antibodies on the ICAM-1-immobilized substrate was examined. Data indicated that this antibody absorption was significantly abolished by incubating abundant

https://doi.org/10.1021/acsami.3c00288
ACS Appl. Mater. Interfaces 2023, 15, 17577−17591

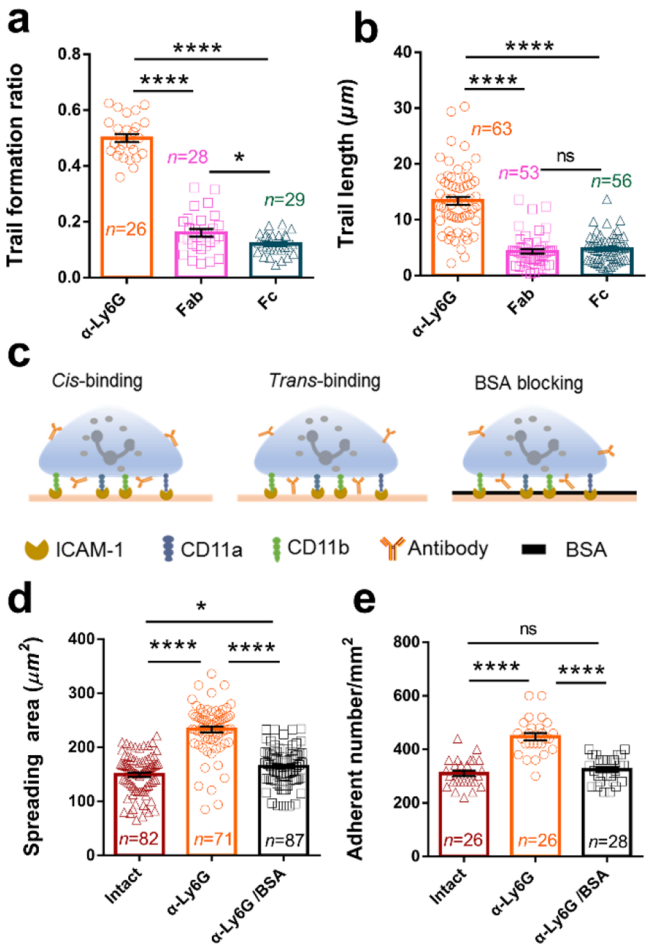

Figure 4. Enhanced trail formation attributes to *trans*-binding of α-Ly6G antibodies. (a, b) Trail formation ratio (a) and length (b) for neutrophils treated by whole α-Ly6G antibodies and their Fab or Fc fragments, respectively. (c) Schematic of distinct binding manners of α-Ly6G antibodies to neutrophils. (d, e) Comparisons of cell spreading area (d) and adhesion number (e) for α-Ly6G-stained neutrophils between the cases of ICAM-1 immobilization alone and the one by incubating abundant BSA (5%) right after immobilizing ICAM-1s on the substrate. Intact cells served as control. Data were obtained from at least three repeats and presented as the mean ± SEM; $p < 0.05^{*}$, 0.0001^{****}.

BSA right after immobilizing ICAM-1 on coverslips, where only barely free sites on the substrate were available for sequent physical absorption of α-Ly6G antibodies (Figure S15d). As predicted, the number and spreading area of adhered neutrophils were significantly reduced by BSA preblocking (Figure 4d,e), together with the lowered trail length, formation ratio, and area as well as uropod length, which were similar to those for intact cells (Figure S16a−d). These results indicated that the trail formation of α-Ly6G-stained neutrophils was likely governed by *trans*-binding of α-Ly6G antibodies absorbed on the ICAM-1 substrate. Evidently, this *trans*-binding manner was also able to enhance neutrophil adhesion and elevated β_2-integrin expression (Figure 3a), leading to a specialized migration strategy for relieving the excessive adhesion and persisting the efficient migration. In contrast, those *cis*-bindings of α-Ly6G antibodies may not work in this way. As seen from the flow cytometry analysis, where soluble α-Ly6G antibodies can only bind to neutrophils in a *cis*-binding manner, no significant difference was observed for β_2-integrin expression between intact and α-Ly6G-stained neutrophils (Figure S16e,f), as expected.

Moreover, these *trans*-binding effects of specific antibodies against neutrophils on inducing trail formation could also be biologically applicable. Here, we replaced α-Ly6G antibodies by α-CD11b antibodies because CD11b is a major cellular adhesive receptor to the ICAM-1 ligand on the neutrophil surface and blocking CD11b did not affect neutrophil migration (Figure S14a−d). Similarly, α-CD11b staining resulted in indifferent migrating trajectories and velocities between intact and α-CD11b-stained neutrophils (Figure S17a−c). As predicted, α-CD11b staining was also able to promote typical trail formation (Figure S17d), with the enhanced cell adhesion number and spreading area (Figure S17e,f) and the increased trail length, formation ratio, area, as well as uropod length (Figure S18a−d), compared with those for intact cells or cells stained with isotype-matched IgG2a staining. Because the above trail parameters and average migrating velocity were remarkably similar to those for α-Ly6G staining (Figure S5b−e, Figure 2a−c), this *trans*-binding manner of neutrophil-specific antibodies could induce neutrophil trail formation, mainly attributed to the excessive adhesion-induced switching of the cell migration strategy.

Neutrophil Trails Act as Immune Forerunners to Recruit DCs. Neutrophil trails are both chemotactic and haptotactic cues, thereby creating a chemoattractive milieu such as CXCL12 for T-cell recruitment.[8] Because those membrane patches derived from migrating neutrophils cannot be directly sensed by T cells,[8] it is still unclear how these chemokines are liberated from the trails and what the subsequent fate of the trails is after neutrophils migrate away from the sites. Here, we simply tested the roles of neutrophil trails in recruiting dendritic cells (DCs) by considering their special roles in patrolling peripheral tissues and initiating lymphocyte responses.[45] Results indicated that DCs tended to be accumulated in the trail-enriched zone when they migrated together with α-Ly6G-stained neutrophils (Figure S19a,b) compared to those without preperfused neutrophils or with preperfused intact neutrophils. Direct physical interactions were observed between DCs and neutrophil trails, where DCs tended to adhere onto the trails rather than the cell body (Figure S19c). Time-lapsed imaging also showed that DCs were able to approach and endocytose the trails at the late stage (Figure S19d, Video S3), which could contribute to chemokine liberation.

On the basis of the observations that DCs tended to be accumulated in the trail-enriched zone (Figure S19), a transwell assay was thus applied to confirm the effect of trails *in vitro* and to determine the optimal trail concentration on recruiting DCs, as it was seen that 50−100 μg of trails could saturate the fraction of DC recruitment in the current setting (Figure 5b). To further verify the effects of trails on recruiting DCs *in vivo*, a hydrogel delivery system was constructed to incorporate the isolated trails with the injectable alginate hydrogel from the material standpoint (Figure 5a) because the alginate hydrogel is widely used as a typical controlled-release carrier of multiple bioactive cytokines due to its biocompatibility, nonthrombogenic nature, mild gelation process, and resemblance to the extracellular matrix.[46] A simple controlled-release test of incorporated trails in alginate hydrogels (Figure 5c) first indicated that the presence of the alginate hydrogel helped to retain the trail concentration and could serve as a temporary repository for the continuous release of trails. Next,

https://doi.org/10.1021/acsami.3c00288
ACS Appl. Mater. Interfaces 2023, 15, 17577−17591

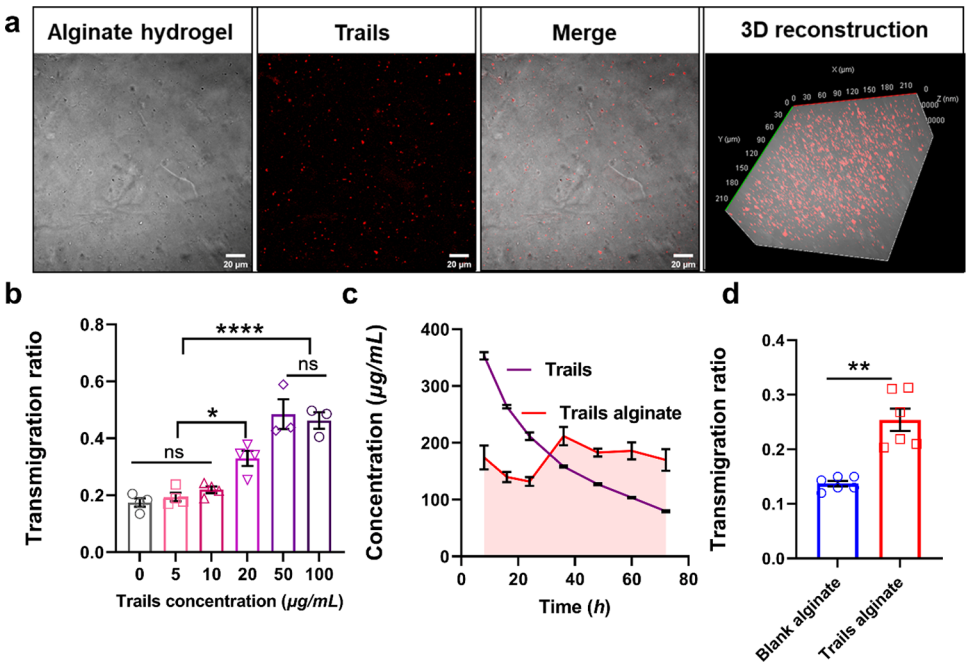

Figure 5. Alginate hydrogels incorporated with trails promote DCs recruitment *in vitro*. (a) Representative images of trails incorporated with the injectable alginate hydrogel. From left to right: the bright-field image of the alginate hydrogel, fluorescence staining of trails (*red*), merged images, and 3D reconstruction images, respectively. (b) Transwell analysis for DC chemotaxis where DCs were seeded on the upper chamber and trails were placed into the lower chamber. (c) Controlled release of trails incorporated into alginate hydrogels. (d) Transwell analysis for DC chemotaxis where DCs were seeded on the upper chamber and the alginate hydrogel was applied alone or incorporated with trails in the lower chamber. Data were obtained from at least three repeats and presented as the mean ± SEM; $p < 0.01^{**}$, $p < 0.0001^{****}$.

the *in vitro* transwell assay was conducted again to confirm the chemotactic effects of the trails in alginate hydrogels (100 μg of trails in 100 μL of hydrogels) on recruiting DCs using (Figure 5d), confirming that the trails in alginate hydrogels could significantly increase DC recruitment *in vitro*.

Finally, the *in vivo* subcutaneous injection experiments into a mouse were conducted to verify the effect of trails on recruiting DCs using 100 μL of blank alginate hydrogels or 100 μg of trails incorporated into alginate hydrogels (100 μg of trails in 100 μL of hydrogels) (Figure 6a,b). Considering the kinetics of DC recruitment *in vivo*,[47,48] the number of APC-CD11c-labeled DCs[49] recruited at hydrogel injection sites at 48 h was increased in trails-incorporated alginate hydrogels compared to blank ones, as observed (Figure 6c) or as statistically analyzed (Figure 6d). Simultaneously, flow cytometry tests were also performed to figure out the ratio of DCs to leukocytes by staining the whole set of collected leukocytes with FITC-CD45.[50,51] Results indicated that the ratio of DCs to leukocytes increased slightly in trails-incorporated alginate hydrogels (Figure 6e,f), suggesting that the delivery of trails-incorporated alginate hydrogel tends to enhance the recruitment of immune cells, especially the DCs.

DISCUSSION

We reported in this study that migrating neutrophils leave behind long-lasting, β_2-integrin-enriched, chemokine-containing membrane remnants settled on the ICAM-1-immobilized substrate *in vitro* or even on the mouse liver endothelium *in vivo*. Although different fractions of CD11a and CD11b are lost during neutrophil migration, actin and focal adhesion proteins remain associated on the cell body and appear to be retained during membrane ripping. In this process, CD11a is clustered and tightly linked to the cytoskeleton to mediate neutrophil migration. Highly expressed CD11b is polarized to the uropod *via* molecular diffusion and enhances adhesion on ICAM-1, increasing the difficulty of rear detachment during cell migration. When cytoskeletal contractility exceeds adhesive strength at the focal contacts, the contractile forces might promote rear detachment from the substrate by membrane ripping, where weak β_2-integrin−cytoskeleton linkage could be disrupted to allow the cell locomotion and the formation of β_2-integrin-enriched trail. In this regard, CD11a is less pulled down from the cell body because it is tightly bound to the cytoskeleton, whereas CD11b is more pulled down because it is loosely bound to the cytoskeletal backbone. As the trails are detached from migrating neutrophils and then attached to the endothelium, neutrophil migration and trail formation are accompanied by intermittent bond formation between specific neutrophil receptors and endothelial ligands.[8,9,32] Thus, trail formation is closely related to cell adhesion and deadhesion during cell migration.

Trail formation is favorable to maintain successive, efficient neutrophil migration. Evidence in this study indicated that neutrophil trails are integrin-enriched, membrane-covered structures. Thus, the release of the trails might serve as a supplemental strategy for rear detachment, allowing efficient cell migration especially based on the enhanced adhesion (Figure 2 and Figure S11). In fact, the loss of vast amounts of integrins from a cell adhered onto the substrate appears to be an efficient way for rear detachment. To sustain neutrophil migration for prolonged periods, the cell must compensate for the loss of cellular integrins and membranes with the synthesis of new integrins and membranes, which could be feasible for neutrophils. For example, fMLP-stimulated neutrophils undergo a transient change in membrane quantities, yielding a 25% component increase of the outer membrane.[52] This membrane

https://doi.org/10.1021/acsami.3c00288
ACS Appl. Mater. Interfaces 2023, 15, 17577−17591

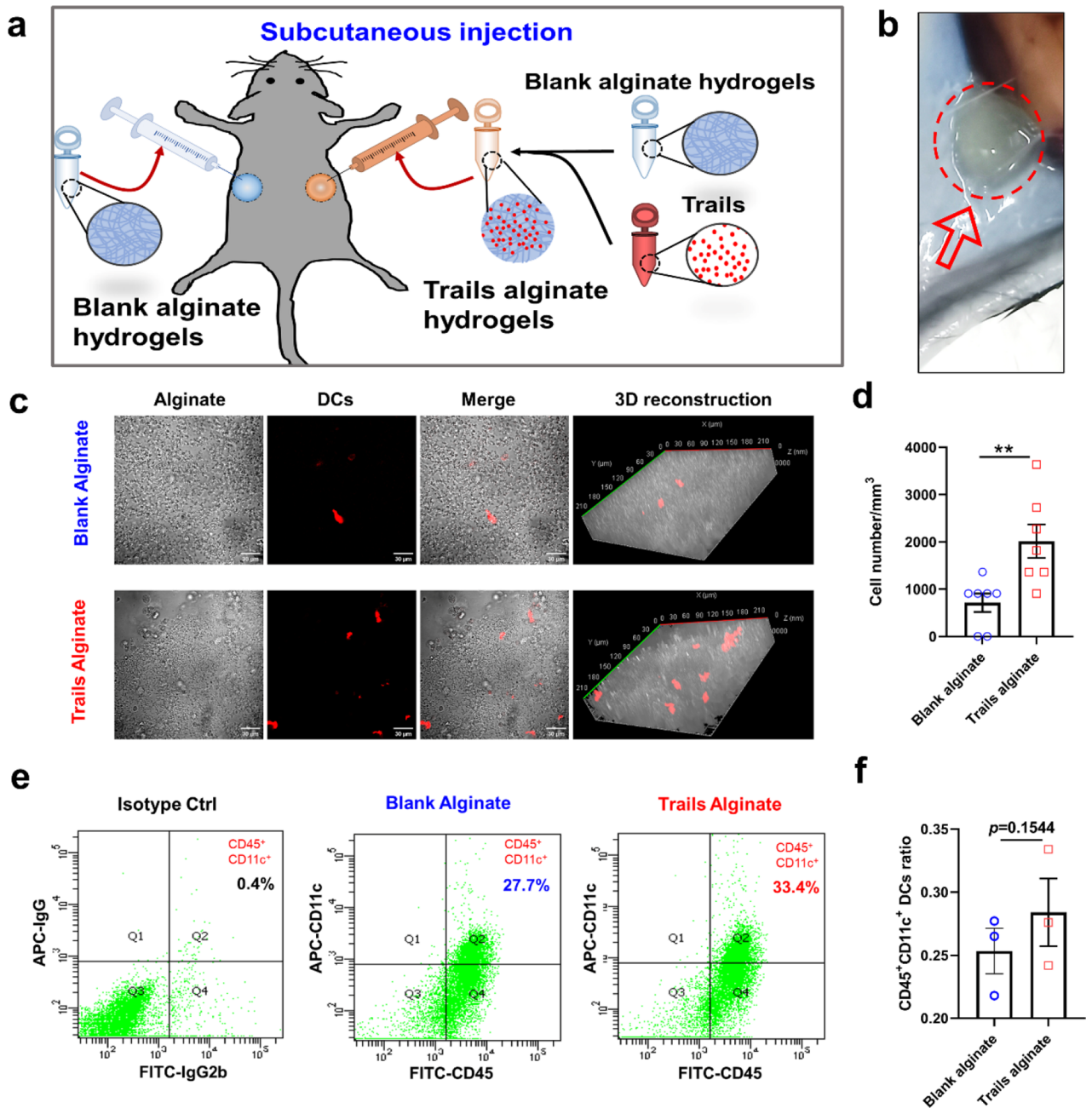

Figure 6. Alginate hydrogels incorporated with trails promote DC recruitment *in vivo*. (a) Schematic of the *in vivo* experiments with the injectable alginate hydrogel delivery system. (b) Alginate hydrogel *in vivo* at 48 h postinjection. (c) Immunofluorescent staining of DCs at 48 h postinjection. From left to right: the bright-field image of alginate hydrogel, fluorescence staining of DCs (*red*), merged images, and 3D reconstruction images, respectively. (d) Statistical analysis of DC number at 48 h postinjection. (e) Scattered plots of flow cytometry analysis of leukocytes harvested at injection sites of alginate hydrogels. Cells were labeled by FITC-CD45 and APC-CD11c. (f) Ratios of DCs to leukocytes at 48 h postinjection. Data were obtained from at least three repeats and presented as the mean ± SEM; $p < 0.01$**.

increase occurs within 10 s after adding the stimulus and corresponds to the disappearance of specific granules and granular membranes from the cytoplasm.[52] These observations suggest that the membrane of neutrophils is redundant to support the formation of such a membranous structure when necessary. Moreover, the subsequent cell migration after trail release possesses a similar average migrating velocity but differential instantaneous edge velocity between the cell frontmost and rearmost, consistent with those polarized distributions of CD11a and CD11b (Figures 2 and 3). This specialized strategy enables neutrophils to alleviate excessive adhesion, which is mainly governed by myosin-II-mediated rear-end retraction and contributes to neutrophil trail formation based on high-instantaneous velocity rear contraction.

Because actin and the related focal adhesion proteins contribute to the formation of focal contacts that are linked to the cytosolic domains of integrins, their distributions at the cell rear are thus critical in trail formation. As shown in Figures S1 and S2, the membranous trails derived from migrating neutrophils are β_2-integrin-enriched, closed structures and short of F-actin and focal adhesion proteins, implying that they

https://doi.org/10.1021/acsami.3c00288
ACS Appl. Mater. Interfaces 2023, 15, 17577−17591

might derive from the dissociation of those cytosolic adapter proteins from the integrins and the discard of those molecular complexes attached to their ECM ligands at the cell rear. In fact, this process usually occurs at high adhesiveness, as reported in the literature.[53,54] Cell migration is highly related to force generation and momentum transfer,[55] and the mechanical forces involved are mostly generated by actomyosin.[56] In this study, α-Ly6G staining significantly increases the adhesiveness between neutrophils and the substrate (Figure 3a−c), which in turn rips down β_2-integrins from the cell membrane based on myosin-mediated uropod contraction and promotes trail formation *via* integrin−cytoskeleton dissociation. Moreover, several morphological parameters were also defined in this study not only for quantifying the trails so formed but also for depicting their underlying biophysical cues. Whereas the trail formation ratio indicates the ensemble capability of migrating neutrophils to form the trails, the trail length and trail area show the size of the trails formed from individual cells. Uropod length not only is used to measure the subcellular geometry at the cell rear but also could represent the strenuous level of rear-end retraction during cell migration.[38]

Integrins mediate physical binding between neutrophils and endothelial cells, which is crucial for generating neutrophil trails.[23,26] The β_2-integrins (also known as CD18), *i.e.*, CD11a/CD18 and CD11b/CD18, are central players in this process. These integrins are expressed on the surface of most leukocytes and regulate leukocyte adhesion and recruitment to damaged or infected tissues during inflammation.[57] Circulating leukocytes usually maintain their integrins in inactive states and undergo *in situ* activation to promote high binding affinity and adhesiveness to their specific endothelial ligands such as ICAM-1.[58] Meanwhile, integrins are manipulated in distinct aspects including intracellular translocation,[59] affinity change, and avidity alteration.[60] For example, the binding affinity of CD11b/CD18 is dynamically regulated through their conformational change,[61,62] and the activity of CD11a/CD18 appears to be mediated largely by their clustering on the membrane, which increases avidity.[63] Evidently, CD11a/CD18 and CD11b/CD18 play different roles in neutrophil chemotactic migration.[64]

This trail formation is also associated with distinct spatial organizations of CD11a and CD11b during neutrophil migration, leading to the dominance of CD11a-mediated cell migration in trail formation (Figure 3d−f and Figure S13). In fact, CD11a can redistribute into dense high-affinity clusters to strengthen adhesion and transduce outside-in signals based on the engagement with ICAM-1.[65] High-affinity CD11a binding to ICAM-1 is required for F-actin-supported cell polarization and transmigration. The cellular cytoskeleton can regulate CD11a avidity by increasing its mobility during activation and directing the motility of CD11a microclusters following ligand engagement. In this study, α-Ly6G or α-CD11b (Figure 4d,e and Figure S17e,f) staining is found to enhance cell adhesion to the substrate and results in a high expression of CD11b (Figure 3*a*), indicating the high effectiveness of CD11b by combining the enhanced expression and polarized location, in addition to the above observations for CD11a in the literature.

These neutrophil trails so formed could be biologically relevant. On the one hand, the trail formation can be induced by β_2-integrin−ICAM-1 binding (Figure 3 and Figure S13). α-Ly6G staining can remarkably enhance the level of ICAM-1-induced trail formation (Figures 1 and 4, Figures S1 and S13) *via* fostering cell adhesion, and these neutrophil trails are able to promote DC recruitment in the *in vitro* model (Figure S19). These observations provide potential molecular targets in regulating neutrophil migration and DC recruitment. On the other hand, the *trans*-binding of specific antibodies seems favorable for cell migration or recruitment *via* enhancing cell adhesion. For example, similar antibody immobilization by precoating a specific antibody onto the scaffold surface emerges as a promising strategy for promoting recruitment of stem cells to scaffolds or biomedical implants, which is meaningful in endothelialization and angiogenesis.[66] Additional evidence is also required to underline the significances of antibody immobilization and cross-linking *in vivo*. For example, the anti-neutrophil cytoplasmic antibody (ANCA)-associated vasculitis is characterized by autoantibodies specific for neutrophil granule components, predominantly proteinase3 (PR3) and myeloperoxidase (MPO) immobilization onto the endothelium.[67,68] Because ANCA has the capacity to activate neutrophils, it could be possible that ANCA binding plays a distinct role in vasculitis through neutrophil trail formation and subsequent immune cells recruitment, as well as propagation of the autoimmune response.

CONCLUSIONS

In this study, migrating neutrophils are found to leave behind long-lasting, chemokine-containing trails settled on the ICAM-1-immobilized substrate *in vitro* or even on the mouse liver endothelium *in vivo*. Trail formation can serve as a migration strategy for cells to discard the excess adhesion by sharp rear contraction and in turn maintain efficient migration with the same migration velocity as intact cells do. Neutrophil trails are not just the byproducts of cell migration, but they also present specialized functions in recruiting DCs to coordinate innate and adaptive immune responses. Delivery of trails that are incorporated into alginate hydrogels provides a novel materials-based approach especially for DCs-based immunotherapy.

ASSOCIATED CONTENT

Supporting Information

The Supporting Information is available free of charge at https://pubs.acs.org/doi/10.1021/acsami.3c00288.

Figure S1 shows the subcellular structures of migrating neutrophil trails. Figure S2 shows the immunofluorescent staining of adhesion molecules and actin binding proteins for α-Ly6G-stained neutrophils on the ICAM-1 substrate. Figure S3 shows the immunofluorescent staining for the isolated trails derived from neutrophils on the ICAM-1 substrate. Figure S4 shows the component identification and morphology distribution for the collected trails derived from neutrophils. Figure S5 shows the subregion definition and morphological analysis for a migrating neutrophil. Figure S6 shows the immunofluorescent staining for intact neutrophils on the ICAM-1 substrate. Figure S7 shows the migration dynamics of intact or α-Ly6G-stained neutrophils on the ICAM-1 substrate. Figure S8 shows that trail formation is positively correlated to cytoskeleton enrichment. Figure S9 shows that neutrophil migration is positively correlated to myosin-II-mediated contraction at the cell rear. Figure S10 shows that inhibition of myosin-II-mediated contraction at the cell rear signifi-

https://doi.org/10.1021/acsami.3c00288
ACS Appl. Mater. Interfaces 2023, 15, 17577−17591

cantly reduces trail formation. Figure S11 shows that trail formation relieves excessive adhesion and maintains efficient cell migration. Figure S12 shows that CD11a but not CD11b associates tightly to the cytoskeleton. Figure S13 shows that CD11a dominates neutrophil trail formation. Figure S14 shows that CD11a dominates neutrophil migration. Figure S15 shows that α-Ly6G *trans*-binding enhances neutrophil trail formation. Figure S16 shows that trail formation is attributed to *trans*-binding of α-Ly6G antibodies. Figure S17 shows that the roles of antibody *trans*-binding in inducing neutrophil migration and spreading are applicable for α-CD11b staining. Figure S18 shows that the roles of antibody *trans*-binding in inducing neutrophil trail formation are applicable for α-CD11b staining. Figure S19 shows that neutrophil-derived β_2-integrin-enriched trails promote DC recruitment. Table S1 shows the trail information by Fourier transform infrared analysis (PDF)

Video S1 shows the migrating neutrophils that deposited the trails on mouse liver sinusoids (MP4)

Video S2 shows the trail formation of α-Ly6G- stained neutrophils on the ICAM-1 substrate (MP4)

Video S3 shows that dendritic cells adhered onto the trails and engulfed the trails at the late stage (MP4)

AUTHOR INFORMATION

Corresponding Authors

Yan Zhang − *Center for Biomechanics and Bioengineering, Key Laboratory of Microgravity (National Microgravity Laboratory) and Beijing Key Laboratory of Engineered Construction and Mechanobiology, Institute of Mechanics, Chinese Academy of Sciences, Beijing 100190, China; School of Engineering Science, University of Chinese Academy of Sciences, Beijing 100049, China*; Email: zhangyan@imech.ac.cn

Mian Long − *Center for Biomechanics and Bioengineering, Key Laboratory of Microgravity (National Microgravity Laboratory) and Beijing Key Laboratory of Engineered Construction and Mechanobiology, Institute of Mechanics, Chinese Academy of Sciences, Beijing 100190, China; School of Engineering Science, University of Chinese Academy of Sciences, Beijing 100049, China*; orcid.org/0000-0003-0819-6186; Email: mlong@imech.ac.cn

Authors

Wenhui Hu − *Center for Biomechanics and Bioengineering, Key Laboratory of Microgravity (National Microgravity Laboratory) and Beijing Key Laboratory of Engineered Construction and Mechanobiology, Institute of Mechanics, Chinese Academy of Sciences, Beijing 100190, China; School of Basic Medical Sciences, Guizhou Medical University, Guiyang 550025, P.R. China*; orcid.org/0000-0002-4303-9672

Wenbo Gao − *Center for Biomechanics and Bioengineering, Key Laboratory of Microgravity (National Microgravity Laboratory) and Beijing Key Laboratory of Engineered Construction and Mechanobiology, Institute of Mechanics, Chinese Academy of Sciences, Beijing 100190, China*; orcid.org/0009-0005-3482-7772

Yixin Gong − *Center for Biomechanics and Bioengineering, Key Laboratory of Microgravity (National Microgravity Laboratory) and Beijing Key Laboratory of Engineered Construction and Mechanobiology, Institute of Mechanics, Chinese Academy of Sciences, Beijing 100190, China; School of Engineering Science, University of Chinese Academy of Sciences, Beijing 100049, China*; orcid.org/0000-0001-7681-9619

Pan Guo − *Center for Biomechanics and Bioengineering, Key Laboratory of Microgravity (National Microgravity Laboratory) and Beijing Key Laboratory of Engineered Construction and Mechanobiology, Institute of Mechanics, Chinese Academy of Sciences, Beijing 100190, China; School of Engineering Science, University of Chinese Academy of Sciences, Beijing 100049, China*; orcid.org/0009-0006-8543-8272

Wang Li − *Center for Biomechanics and Bioengineering, Key Laboratory of Microgravity (National Microgravity Laboratory) and Beijing Key Laboratory of Engineered Construction and Mechanobiology, Institute of Mechanics, Chinese Academy of Sciences, Beijing 100190, China; School of Engineering Science, University of Chinese Academy of Sciences, Beijing 100049, China*; orcid.org/0009-0004-6663-9955

Xinyu Shu − *Center for Biomechanics and Bioengineering, Key Laboratory of Microgravity (National Microgravity Laboratory) and Beijing Key Laboratory of Engineered Construction and Mechanobiology, Institute of Mechanics, Chinese Academy of Sciences, Beijing 100190, China; School of Engineering Science, University of Chinese Academy of Sciences, Beijing 100049, China*; orcid.org/0009-0009-6992-8513

Shouqin Lü − *Center for Biomechanics and Bioengineering, Key Laboratory of Microgravity (National Microgravity Laboratory) and Beijing Key Laboratory of Engineered Construction and Mechanobiology, Institute of Mechanics, Chinese Academy of Sciences, Beijing 100190, China; School of Engineering Science, University of Chinese Academy of Sciences, Beijing 100049, China*

Zhu Zeng − *School of Basic Medical Sciences, Guizhou Medical University, Guiyang 550025, P.R. China*; orcid.org/0000-0003-1989-5142

Complete contact information is available at: https://pubs.acs.org/10.1021/acsami.3c00288

Author Contributions

M.L., Y.Z., W.H.H., and Y.X.G designed the project; W.H.H., P.G., W.B.G., W.L., and X.Y.S. performed the experiments; W.H.H, Y.Z., Z.Z., W.B.G., W.L., and S.Q.L. analyzed the data; M.L., Y.Z., and W.H.H. wrote the manuscript.

Notes

The authors declare no competing financial interest.

ACKNOWLEDGMENTS

We thank Y. Xia for technical assistance with FTIR and data analysis. We are also grateful to P. Li for assistances with mouse experiments and D. Huang with immunofluorescence imaging. This work was supported by the National Natural Science Foundation of China grants 32130061, 12272389, and 11772345; Scientific Instrument Developing Project of the Chinese Academy of Sciences grant GJJSTU20220002; and Frontier Science Key Project of Chinese Science Academy grant QYZDJ-SSW-JSC018.

REFERENCES

(1) Fine, N.; Tasevski, N.; McCulloch, C. A.; Tenenbaum, H. C.; Glogauer, M. The Neutrophil: Constant Defender and First Responder. *Front. Immunol.* **2020**, *11*, 571085.

(2) Thieblemont, N.; Wright, H. L.; Edwards, S. W.; Witko-Sarsat, V. Human Neutrophils in Auto-immunity. *Semin. Immunol.* **2016**, *28*, 159−173.

(3) Silvestre-Roig, C.; Braster, Q.; Ortega-Gomez, A.; Soehnlein, O. Neutrophils as Regulators of Cardiovascular Inflammation. *Nat. Rev. Cardiol.* **2020**, *17*, 327−340.

(4) Nourshargh, S.; Alon, R. Leukocyte Migration into Inflamed Tissues. *Immunity* **2014**, *41*, 694−707.

(5) Filippi, M. D. Neutrophil Transendothelial Migration: Updates and New Perspectives. *Blood* **2019**, *133*, 2149−2158.

(6) Kolaczkowska, E.; Kubes, P. Neutrophil Recruitment and Function in Health and Inflammation. *Nat. Rev. Immunol.* **2013**, *13*, 159−175.

(7) Rosales, C. Neutrophils at the Crossroads of Innate and Adaptive Immunity. *J. Leukocyte Biol.* **2020**, *108*, 377−396.

(8) Lim, K.; Hyun, Y. M.; Lambert-Emo, K.; Capece, T.; Bae, S.; Miller, R.; Topham, D. J.; Kim, M. Neutrophil Trails Guide Influenza-Specific $CD8^+$ T Cells in the Airways. *Science* **2015**, *349*, aaa4352.

(9) Youn, Y. J.; Shrestha, S.; Lee, Y. B.; Kim, J. K.; Lee, J. H.; Hur, K.; Mali, N. M.; Nam, S. W.; Kim, S. H.; Lee, S.; Song, D. K.; Jin, H. K.; Bae, J. S.; Hong, C. W. Neutrophil-Derived Trail is a Proinflammatory Subtype of Neutrophil-Derived Extracellular Vesicles. *Theranostics* **2021**, *11*, 2770−2787.

(10) Sekheri, M.; Othman, A.; Filep, J. G. β_2 Integrin Regulation of Neutrophil Functional Plasticity and Fate in the Resolution of Inflammation. *Front. Immunol.* **2021**, *12*, 660760.

(11) Bouti, P.; Webbers, S. D. S.; Fagerholm, S. C.; Alon, R.; Moser, M.; Matlung, H. L.; Kuijpers, T. W. β_2 Integrin Signaling Cascade in Neutrophils: More Than a Single Function. *Front. Immunol.* **2021**, *11*, 619925.

(12) Anderson, D. C.; Schmalsteig, F. C.; Finegold, M. J.; Hughes, B. J.; Rothlein, R.; Miller, L. J.; Kohl, S.; Tosi, M. F.; Jacobs, R. L.; Waldrop, T. C.; Goldman, A. S.; Shearer, W. T.; Springer, T. A. The Severe and Moderate Phenotypes of Heritable Mac-1, LFA-1 Deficiency: Their Quantitative Definition and Relation to Leukocyte Dysfunction and Clinical Features. *J. Infect. Dis.* **1985**, *152*, 668−689.

(13) Morikis, V. A.; Simon, S. I. Neutrophil Mechanosignaling Promotes Integrin Engagement With Endothelial Cells and Motility Within Inflamed Vessels. *Front. Immunol.* **2018**, *9*, 2774.

(14) El Kebir, D.; Filep, J. G. Modulation of Neutrophil Apoptosis and the Resolution of Inflammation through β_2 Integrins. *Front. Immunol.* **2013**, *4*, 60.

(15) Li, N.; Yang, H.; Wang, M.; Lü, S.; Zhang, Y.; Long, M. Ligand-Specific Binding Forces of LFA-1 and Mac-1 in Neutrophil Adhesion and Crawling. *Mol. Biol. Cell* **2018**, *29*, 408−418.

(16) Buffone, A., Jr.; Anderson, N. R.; Hammer, D. A. Human Neutrophils Will Crawl Upstream on ICAM-1 if Mac-1 Is Blocked. *Biophys. J.* **2019**, *117*, 1393−1404.

(17) Neelamegham, S.; Taylor, A. D.; Burns, A. R.; Smith, C. W.; Simon, S. I. Hydrodynamic Shear Shows Distinct Roles for LFA-1 and Mac-1 in Neutrophil Adhesion to Intercellular Adhesion Molecule-1. *Blood* **1998**, *92*, 1626−1638.

(18) McDonald, B.; McAvoy, E. F.; Lam, F.; Gill, V.; de la Motte, C.; Savani, R. C.; Kubes, P. Interaction of CD44 and Hyaluronan Is the Dominant Mechanism for Neutrophil Sequestration in Inflamed Liver Sinusoids. *J. Exp. Med.* **2008**, *205*, 915−927.

(19) Menezes, G. B.; Lee, W.-Y.; Zhou, H.; Waterhouse, C. C. M.; Cara, D. C.; Kubes, P. Selective Down-regulation of Neutrophil Mac-1 in Endotoxemic Hepatic Microcirculation via IL-10. *J. Immunol.* **2009**, *183*, 7557−7568.

(20) Shen, Y.; Zhang, W.; Xie, Y.; Li, A.; Wang, X.; Chen, X.; Liu, Q.; Wang, Q.; Zhang, G.; Liu, Q.; Liu, J.; Zhang, D.; Zhang, Z.; Ding, J. Surface Modification to Enhance Cell Migration on Biomaterials and Its Combination with 3D Structural Design of Occluders to Improve Interventional Treatment of Heart Diseases. *Biomaterials* **2021**, *279*, 121208.

(21) Ciobanasu, C.; Faivre, B.; Le Clainche, C. Integrating Actin Dynamics, Mechanotransduction and Integrin Activation: The Multiple Functions of Actin Binding Proteins in Focal Adhesions. *Eur. J. Cell Biol.* **2013**, *92*, 339−348.

(22) He, J.; Shen, R.; Liu, Q.; Zheng, S.; Wang, X.; Gao, J.; Wang, Q.; Huang, J.; Ding, J. RGD Nanoarrays with Nanospacing Gradient Selectively Induce Orientation and Directed Migration of Endothelial and Smooth Muscle Cells. *ACS Appl. Mater. Interfaces* **2022**, *14*, 37436−37446.

(23) Yu, Y.; Wang, X.; Zhu, Y.; He, Y.; Xue, H.; Ding, J. Is Polydopamine Beneficial for Cells on the Modified Surface? *Regener. Biomater.* **2022**, *9*, rbac078.

(24) Carvalho, K.; Lemière, J.; Faqir, F.; Manzi, J.; Blanchoin, L.; Plastino, J.; Betz, T.; Sykes, C. Actin Polymerization or Myosin Contraction: Two Ways to Build up Cortical Tension for Symmetry Breaking. *Philos. Trans. R. Soc., B* **2013**, *368*, 20130005.

(25) Hind, L. E.; Vincent, W. J. B.; Huttenlocher, A. Leading from the Back: The Role of the Uropod in Neutrophil Polarization and Migration. *Dev. Cell* **2016**, *38*, 161−169.

(26) Hirata, H.; Sokabe, M.; Lim, C. T. Molecular Mechanisms Underlying the Force-Dependent Regulation of Actin-to-ECM Linkage at the Focal Adhesions. *Prog. Mol. Biol. Transl. Sci.* **2014**, *126*, 135−154.

(27) Chen, W. T. Mechanism of Retraction of the Trailing Edge During Fibroblast Movement. *J. Cell Biol.* **1981**, *90*, 187−200.

(28) Rigort, A.; Grünewald, J.; Herzog, V.; Kirfel, G. Release of Integrin Macroaggregates as a Mechanism of Rear Detachment During Keratinocyte Migration. *Eur. J. Cell Biol.* **2004**, *83*, 725−733.

(29) Führ, G.; Richter, E.; Zimmermann, H.; Hitzler, H.; Niehus, H.; Hagedorn, R. Cell Traces-Footprints of Individual Cells During Locomotion and Adhesion. *Biol. Chem.* **1998**, *379*, 1161−1174.

(30) Palecek, S. P.; Huttenlocher, A.; Horwitz, A. F.; Lauffenburger, D. A. Physical and Biochemical Regulation of Integrin Release During Rear Detachment of Migrating Cells. *J. Cell Sci.* **1998**, *111*, 929−940.

(31) Kirfel, G.; Rigort, A.; Borm, B.; Herzog, V. Cell Migration: Mechanisms of Rear Detachment and the Formation of Migration Tracks. *Eur. J. Cell Biol.* **2004**, *83*, 717−724.

(32) Hyun, Y. M.; Sumagin, R.; Sarangi, P. P.; Lomakina, E.; Overstreet, M. G.; Baker, C. M.; Fowell, D. J.; Waugh, R. E.; Sarelius, I. H.; Kim, M. Uropod Elongation is a Common Final Step in Leukocyte Extravasation Through Inflamed Vessels. *J. Exp. Med.* **2012**, *209*, 1349−1362.

(33) Huang, D.; Ding, Q.; Chen, S.; Lü, S.; Zhang, Y.; Long, M. E-selectin Negatively Regulates Polymorphonuclear Neutrophil Transmigration Through Altered Endothelial Junction Integrity. *FASEB J.* **2021**, *35*, No. e21521.

(34) Sprague, B. L.; McNally, J. G. FRAP Analysis of Binding: Proper and Fitting. *Trends Cell Biol.* **2005**, *15*, 84−91.

(35) Comrie, W. A.; Li, S.; Boyle, S.; Burkhardt, J. K. The Dendritic Cell Cytoskeleton Promotes T Cell Adhesion and Activation by Constraining ICAM-1 Mobility. *J. Cell Biol.* **2015**, *208*, 457−473.

(36) Kuo, C. K.; Ma, P. X. Ionically Crosslinked Alginate Hydrogels as Scaffolds for Tissue Engineering: Part 1. Structure, Gelation Rate and Mechanical Properties. *Biomaterials* **2001**, *22*, 511−521.

(37) Roncada, T.; Bonithon, R.; Blunn, G.; Roldo, M. Soft Substrates Direct Stem Cell Differentiation into the Chondrogenic Lineage Without the Use of Growth Factors. *J. Tissue Eng.* **2022**, *13*, 20417314221122121.

(38) Wang, J.; Hossain, M.; Thanabalasuriar, A.; Gunzer, M.; Meininger, C.; Kubes, P. Visualizing the Function and Fate of Neutrophils in Sterile Injury and Repair. *Science* **2017**, *358*, 111−116.

(39) Tong, C. F.; Zhang, Y.; Lü, S. Q.; Li, N.; Gong, Y. X.; Yang, H.; Feng, S. L.; Du, Y.; Huang, D. D.; Long, M. Binding of Intercellular Adhesion Molecule 1 to β_2-Integrin Regulates Distinct Cell Adhesion Processes on Hepatic and Cerebral Endothelium. *Am. J. Physiol.: Cell Physiol.* **2018**, *315*, 409−421.

https://doi.org/10.1021/acsami.3c00288
ACS Appl. Mater. Interfaces 2023, 15, 17577−17591

(40) Margraf, A.; Ley, K.; Zarbock, A. Neutrophil Recruitment: From Model Systems to Tissue-Specific Patterns. *Trends Immunol.* **2019**, *40*, 613−634.
(41) Puleo, J. I.; Parker, S. S.; Roman, M. R.; Watson, A. W.; Eliato, K. R.; Peng, L.; Saboda, K.; Roe, D. J.; Ros, R.; Gertler, F. B.; Mouneimne, G. Mechanosensing During Directed Cell Migration Requires Dynamic Actin Polymerization at Focal Adhesions. *J. Cell Biol.* **2019**, *218*, 4215−4235.
(42) Liu, Q.; Zheng, S.; Ye, K.; He, J.; Shen, Y.; Cui, S.; Huang, J.; Gu, Y.; Ding, J. Cell Migration Regulated by RGD Nanospacing and Enhanced Under Moderate Cell Adhesion on Biomaterials. *Biomaterials* **2020**, *263*, 120327.
(43) Cramer, L. P.; Kay, R. R.; Zatulovskiy, E. Repellent and Attractant Guidance Cues Initiate Cell Migration by Distinct Rear-Driven and Front-Driven Cytoskeletal Mechanisms. *Curr. Biol.* **2018**, *28*, 995−1004.e3.
(44) He, J.; Liu, Q.; Zheng, S.; Shen, R.; Wang, X.; Gao, J.; Wang, Q.; Huang, J.; Ding, J. Enlargement, Reduction, and even Reversal of Relative Migration Speeds of Endothelial and Smooth Muscle Cells on Biomaterials Simply by Adjusting RGD Nanospacing. *ACS Appl. Mater. Interfaces* **2021**, *13*, 42344−42356.
(45) Liu, J.; Zhang, X.; Cheng, Y.; Cao, X. Dendritic Cell Migration in Inflammation and Immunity. *Cell. Mol. Immunol.* **2021**, *18*, 2461−2471.
(46) Ruvinov, E.; Cohen, S. Alginate Biomaterial for the Treatment of Myocardial Infarction: Progress, Translational Strategies, and Clinical Outlook: From Ocean Algae to Patient Bedside. *Adv. Drug Delivery Rev.* **2016**, *96*, 54−76.
(47) Yang, W.; Tao, Y.; Wu, Y.; Zhao, X.; Ye, W.; Zhao, D.; Fu, L.; Tian, C.; Yang, J.; He, F.; Tang, L. Neutrophils Promote the Development of Reparative Macrophages Mediated by ROS to Orchestrate Liver Repair. *Nat. Commun.* **2019**, *10*, 1076.
(48) Hu, W.; Wang, Y.; Chen, J.; Yu, P.; Tang, F.; Hu, Z.; Zhou, J.; Liu, L.; Qiu, W.; Ye, Y.; Jia, Y.; Zhou, S.; Long, J.; Zeng, Z. Regulation of Biomaterial Implantation-Induced Fibrin Deposition to Immunological Functions of Dendritic Cells. *Mater. Today Bio* **2022**, *14*, 100224.
(49) Singh-Jasuja, H.; Thiolat, A.; Ribon, M.; Boissier, M. C.; Bessis, N.; Rammensee, H. G.; Decker, P. The Mouse Dendritic Cell Marker CD11c Is Down-regulated Upon Cell Activation Through Toll-like Receptor Triggering. *Immunobiology* **2013**, *218*, 28−39.
(50) Zaynagetdinov, R.; Sherrill, T. P.; Kendall, P. L.; Segal, B. H.; Weller, K. P.; Tighe, R. M.; Blackwell, T. S. Identification of Myeloid Cell Subsets in Murine Lungs Using Flow Cytometry. *Am. J. Respir. Cell Mol. Biol.* **2013**, *49*, 180−189.
(51) Martini, E.; Kunderfranco, P.; Peano, C.; Carullo, P.; Cremonesi, M.; Schorn, T.; Carriero, R.; Termanini, A.; Colombo, F. S.; Jachetti, E.; Panico, C.; Faggian, G.; Fumero, A.; Torracca, L.; Molgora, M.; Cibella, J.; Pagiatakis, C.; Brummelman, J.; Alvisi, G.; Mazza, E. M. C.; Colombo, M. P.; Lugli, E.; Condorelli, G.; Kallikourdis, M. Single-Cell Sequencing of Mouse Heart Immune Infiltrate in Pressure Overload-Driven Heart Failure Reveals Extent of Immune Activation. *Circulation* **2019**, *140*, 2089−2107.
(52) Hoffstein, S. T.; Friedman, R. S.; Weissmann, G. Degranulation, Membrane Addition, and Shape Change During Chemotactic Factor-Induced Aggregation of Human Neutrophils. *J. Cell Biol.* **1982**, *95*, 234−241.
(53) DiMilla, P. A.; Barbee, K.; Lauffenburger, D. A. Mathematical Model for the Effects of Adhesion and Mechanics on Cell Migration Speed. *Biophys. J.* **1991**, *60*, 15−37.
(54) Sheetz, M. P. Cell Migration by Graded Attachment to Substrates and Contraction. *Semin. Cell Biol.* **1994**, *5*, 149−155.
(55) Moreau, H. D.; Piel, M.; Voituriez, R.; Lennon-Duménil, A. M. Integrating Physical and Molecular Insights on Immune Cell Migration. *Trends Immunol.* **2018**, *39*, 632−643.
(56) Tsai, T. Y.-C.; Collins, S. R.; Chan, C. K.; Hadjitheodorou, A.; Lam, P. Y.; Lou, S. S.; Yang, H. W.; Jorgensen, J.; Ellett, F.; Irimia, D.; Davidson, M. W.; Fischer, R. S.; Huttenlocher, A.; Meyer, T.; Ferrell, J. E., Jr.; Theriot, J. A. Efficient Front-Rear Coupling in Neutrophil Chemotaxis by Dynamic Myosin II Localization. *Dev. Cell* **2019**, *49*, 189−205.e6.
(57) Thome, S.; Begandt, D.; Pick, R.; Salvermoser, M.; Walzog, B. Intracellular β_2 Integrin (CD11/CD18) Interacting Partners in Neutrophil Trafficking. *Eur. J. Clin. Invest.* **2018**, *48*, No. e12966.
(58) Futosi, K.; Fodor, S.; Mócsai, A. Reprint of Neutrophil Cell Surface Receptors and Their Intracellular Signal Transduction Pathways. *Int. Immunopharmacol.* **2013**, *17*, 1185−1197.
(59) Moreno-Layseca, P.; Icha, J.; Hamidi, H.; Ivaska, J. Integrin Trafficking in Cells and Tissues. *Nat. Cell Biol.* **2019**, *21*, 122−132.
(60) Sun, Z.; Costell, M.; Fässler, R. Integrin Activation by Talin, Kindlin and Mechanical Forces. *Nat. Cell Biol.* **2019**, *21*, 25−31.
(61) Lee, J. O.; Bankston, L. A.; Arnaout, M. A.; Liddington, R. C. Two Conformations of the Integrin A-Domain (I-Domain): A Pathway for Activation? *Structure* **1995**, *3*, 1333−1340.
(62) Rosetti, F.; Chen, Y.; Sen, M.; Thayer, E.; Azcutia, V.; Herter, J. M.; Luscinskas, F. W.; Cullere, X.; Zhu, C.; Mayadas, T. N. A Lupus-Associated Mac-1 Variant Has Defects in Integrin Allostery and Interaction with Ligands Under Force. *Cell Rep.* **2015**, *10*, 1655−1664.
(63) Hogg, N.; Leitinger, B. Shape and Shift Changes Related to the Function of Leukocyte Integrins LFA-1 and Mac-1. *J. Leukocyte Biol.* **2001**, *69*, 893−898.
(64) Heit, B.; Colarusso, P.; Kubes, P. Fundamentally Different Roles for LFA-1, Mac-1 and Alpha4-Integrin in Neutrophil Chemotaxis. *J. Cell Sci.* **2005**, *118*, 5205−5220.
(65) Simon, S. I.; Sarantos, M. R.; Green, C. E.; Schaff, U. Y. Leucocyte Recruitment Under Fluid Shear: Mechanical and Molecular Regulation Within the Inflammatory Synapse. *Clin. Exp. Pharmacol. Physiol.* **2009**, *36*, 217−224.
(66) Pacelli, S.; Basu, S.; Whitlow, J.; Chakravarti, A.; Acosta, F.; Varshney, A.; Modaresi, S.; Berkland, C.; Paul, A. Strategies to Develop Endogenous Stem Cell-Recruiting Bioactive Materials for Tissue Repair and Regeneration. *Adv. Drug Delivery Rev.* **2017**, *120*, 50−70.
(67) Bai, M.; Grieshaber-Bouyer, R.; Wang, J.; Schmider, A. B.; Wilson, Z. S.; Zeng, L.; Halyabar, O.; Godin, M. D.; Nguyen, H. N.; Levescot, A.; Cunin, P.; Lefort, C. T.; Soberman, R. J.; Nigrovic, P. A. CD177 Modulates Human Neutrophil Migration Through Activation-Mediated Integrin and Chemoreceptor Regulation. *Blood* **2017**, *130*, 2092−2100.
(68) Hutton, H. L.; Holdsworth, S. R.; Kitching, A. R. ANCA-Associated Vasculitis: Pathogenesis, Models, and Preclinical Testing. *Semin. Nephrol.* **2017**, *37*, 418−435.

https://doi.org/10.1021/acsami.3c00288
ACS Appl. Mater. Interfaces 2023, 15, 17577−17591